TÜBİTAK

Turkish Journal of Earth Sciences

http://journals.tubitak.gov.tr/earth/

Research Article

Turkish J Earth Sci
(2018) 27: 89-109

doi:10.3906/yer-1706-19

Triassic-Jurassic arc magmatism in the Pontides as revealed by the U-Pb detrital zircon ages in the Jurassic sandstones of northeastern Turkey

Remziye AKDOĞAN[1,2,*], Aral I. OKAY[1,3], István DUNKL[2]

[1]Department of Geology, Faculty of Mines, İstanbul Technical University, Maslak, İstanbul, Turkey
[2]Department of Sedimentology/Environmental Geology, Geoscience Center, University of Göttingen, Göttingen, Germany
[3]Eurasia Institute of Earth Sciences, İstanbul Technical University, Maslak, İstanbul, Turkey

Received: 20.06.2017 • **Accepted/Published Online:** 16.01.2018 • **Final Version:** 19.03.2018

Abstract: The Eastern Pontides were located at the southern active margin of Laurasia during Mesozoic time. Jurassic volcaniclastic sediments and volcanic rocks of the Pontides represent products of the arc magmatism above a north-dipping subduction zone. Despite the wide distribution of the Jurassic volcaniclastic/volcanic succession, the precise age of the Jurassic volcaniclastic sequence and that of the synsedimentary magmatism are poorly constrained. Here we present U-Pb detrital zircon ages from two Jurassic sandstones belonging to the Şenköy Formation of the Eastern Pontides. One sample is taken from the base of the Şenköy Formation unconformably overlying the late Carboniferous Gümüşhane granite. The depositional age of this sandstone is constrained as late Sinemurian-Pliensbachian based on the faunal assemblage of the overlying Ammonitico Rosso type carbonates. Detrital zircon grains from this sample yielded an unexpected component of 203.4 ± 0.2 Ma (Latest Triassic, Rhaetian) U-Pb age, indicating the existence of Late Triassic magmatic activity in the region that has not been reported yet from the exposed magmatic bodies or from the detrital zircon ages. The sample taken from the upper part of the Jurassic succession yielded a youngest U-Pb age component of 155.9 ± 1.8 Ma, indicating that the depositional age of the Jurassic volcaniclastic succession extends from the Early Jurassic (Sinemurian), as revealed by the fossil content and abundant U-Pb detrital zircon ages, to the Late Jurassic (Oxfordian-Kimmeridgian). The detrital zircon ages from this study together with those from the literature indicate arc magmatism on the southern margin of Laurasia during the Triassic and Late Jurassic (250–156 Ma).

Key words: U-Pb zircon ages, Jurassic, Triassic, arc magmatism, provenance, Eastern Pontides, Tethys

1. Introduction

The Pontides were located on the active southern margin of Laurasia during Permo-Triassic and Jurassic time, facing the Tethyan Ocean in the south (e.g., Robertson and Dixon, 1984; Dercourt et al., 1986, 1993; Ustaömer and Robertson, 1993, 1994, 1997; Barrier and Vrielyneck, 2008; Topuz et al., 2013; Okay and Nikishin, 2015). Previous studies (e.g., Okay and Monié, 1997; Okay et al., 2002; Okay and Göncüoğlu, 2004; Topuz et al., 2004, 2014) mentioned Permo-Triassic accretionary complexes, which include greenschist- to blueschist-facies rocks with lenses of eclogites, indicating the presence of a coeval subduction zone. The Permo-Triassic subduction and deformation events in the Pontides are commonly attributed to the Cimmeride Orogeny, leading to closure of the Paleo-Tethys Ocean and opening of the Neo-Tethys (e.g., Şengör, 1984; Stampfli and Borel, 2002). A Permo-Triassic magmatic arc related to coeval subduction has not been documented. However, beneath the Tertiary sedimentary rocks of the Scythian Platform, deep wells indicate the presence of Triassic igneous rocks (details in Okay et al., 2013; Okay and Nikishin, 2015) and were interpreted as parts of the possible Triassic magmatic arc. The Triassic Cimmeride Orogeny was followed by the development of a Jurassic magmatic arc, which can be traced along the Sakarya Zone, Crimea, and the Caucasus (e.g., Şen, 2007; Nzegge, 2008; Dokuz et al., 2010; Genç and Tüysüz, 2010; Meijers et al., 2010; Adamia et al., 2011; Okay et al., 2014; Okay and Nikishin, 2015). During the arc magmatism, the Jurassic Şenköy Formation, composed of mainly volcaniclastics and volcanic rocks with some Ammonitico Rosso type carbonate levels and coal horizons, was deposited in arc-related basins (e.g., Robinson et al., 1995; Kandemir, 2004; Dokuz and Tanyolu, 2006; Kandemir and Yılmaz, 2009; Akdoğan, 2011; Figure 1). The age of the Şenköy Formation is regarded as Sinemurian up to Bathonian on the basis of a wide range of fossil assemblages (Wedding, 1963; Alkaya and Meister, 1995; Robinson et al., 1995;

* Correspondence: remziyeak@gmail.com

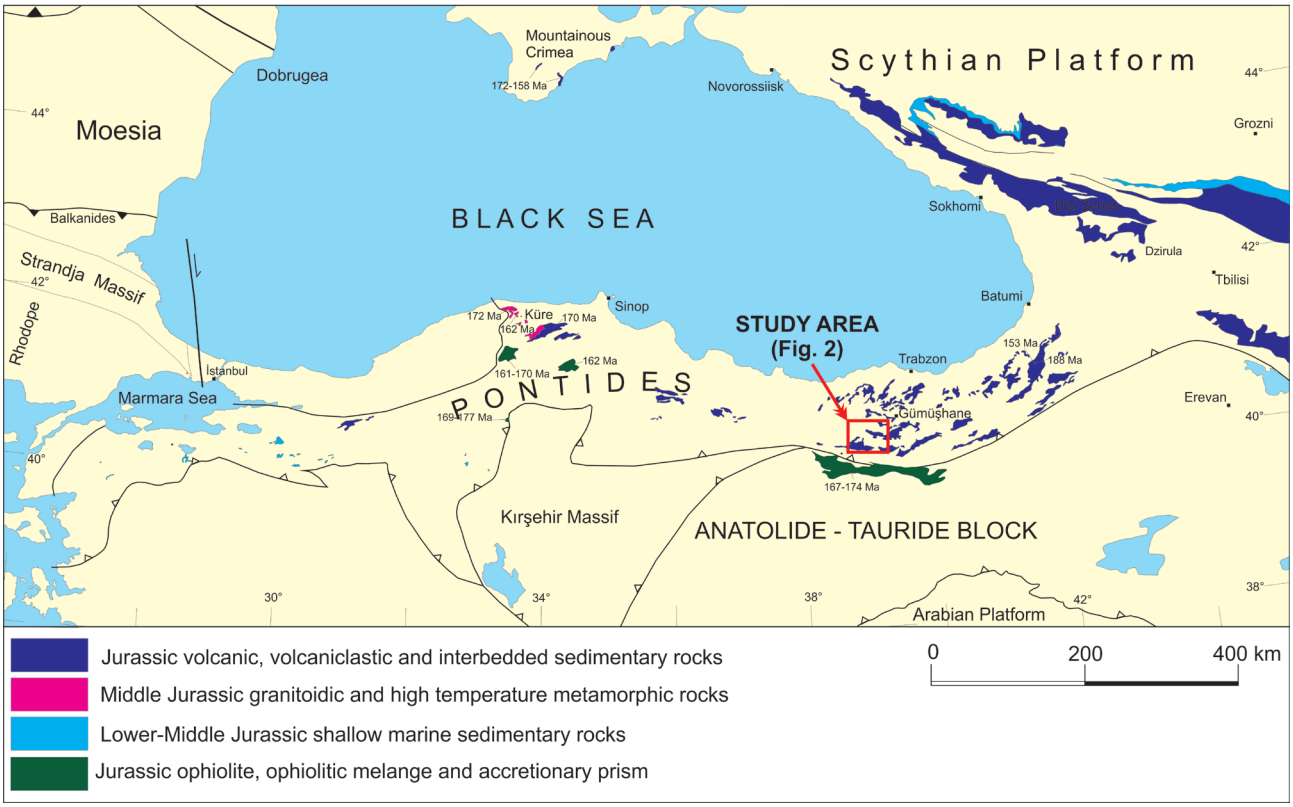

Figure 1. Distribution of the Jurassic rocks in the Black Sea region (modified from Okay and Nikishin, 2015, and references therein). Ar-Ar ages "158 and 188 Ma" are from Dokuz et al. (2010). The study area is marked by a red rectangle.

Kandemir and Yılmaz, 2009; Vörös and Kandemir, 2011). The age of the upper parts of the succession is not well constrained, since the main components in this thickest part are volcaniclastic and volcanic rocks. There are only a few isotopic ages from the Jurassic volcanic and plutonic rocks from the Pontides and Crimea, which range from Pliensbachian to Bathonian (Nzegge, 2008; Dokuz et al., 2010; Meijers et al., 2010; Okay et al., 2014; Figure 1).

In this paper we provide the first U-Pb detrital zircon ages from Jurassic sandstones of the Şenköy Formation in the Eastern Pontides and discuss the provenance of the succession and the Jurassic and earlier magmatism in the region.

2. Pre-Jurassic basement rocks of the Pontides

The Pontide orogenic belt is the northernmost tectonic unit of Turkey, bordered by the Black Sea in the north, and it is separated from the Anatolide-Tauride Block by the İzmir-Ankara-Erzincan Suture in the south (Okay and Tüysüz, 1999; Figure 1). The collision of these two blocks occurred during the Paleocene to Early Eocene (Okay and Şahintürk, 1997; Okay and Tüysüz, 1999). The Pontides consist of three major tectonic zones: the Rhodope-Strandja, İstanbul, and Sakarya zones. The Sakarya Zone is the main tectonic unit of the Pontides, extending 1500 km north of the İzmir-Ankara-Erzincan Suture. The pre-Jurassic basement rocks of the Sakarya Zone are divided into three major units: i) Metamorphic rocks intruded by Carboniferous and Permian granitoids, constituting the Hercynian crystalline basement (e.g., Okay, 1996; Okay et al., 1996, 2006a, 2006b; Topuz et al., 2004, 2007, 2010; Nzegge et al., 2006; Dokuz, 2011; Kaygusuz et al., 2012, 2016; Ustaömer et al., 2012; Ustaömer et al., 2013). Small Devonian intrusions were also described in the western part of the Sakarya Zone by Aysal et al. (2012) and Sunal (2012). ii) Permo-Triassic accretionary complexes, called the Karakaya Complex, subdivided into a lower section made up of metabasites with tectonic slices of Late Triassic eclogite and blueschist facies rocks, and an upper part of chaotically deformed greywackes and basalts with exotic Permo-Carboniferous limestone blocks (Okay and Monié, 1997; Okay et al., 2002; Topuz et al., 2004, 2014). The Triassic Küre Complex in the Central Pontides, consisting of the Upper Triassic Akgöl Flysch with serpentinite, pillow lava, and dolerites (Ustaömer and Robertson, 1994), can be correlated with the Upper Karakaya Complex. The Küre basin is commonly regarded as a back-arc basin (e.g., Ustaömer and Robertson, 1993,

1994; Barrier and Vrielynck, 2008). However, recent study showed that there was no Triassic or older unit between the Küre Complex and the İzmir-Ankara suture and the Küre basin was in a fore-arc position facing the Tethyan Ocean in the south (Okay et al. 2006a, 2006b, 2013, 2014). iii) Nonmetamorphic Permo-Carboniferous sediments from the eastern part of the Sakarya zone (Robinson et al., 1995; Okay and Leven, 1996; Çapkınoğlu, 2003; Kandemir and Lerosey-Aubril, 2011).

Pre-Jurassic basement rocks of the Pontides are unconformably overlain by the Jurassic clastics and volcaniclastics in the Central and Eastern Pontides (e.g., Okay and Şahintürk, 1997; Kandemir, 2004; Şen, 2007; Kandemir and Yılmaz, 2009; Genç and Tüysüz, 2010; Figure 1). The succession includes acidic to intermediate intrusions of Middle Jurassic age in the Central Pontides (details in Yılmaz and Boztuğ, 1986; Nzegge, 2008; Okay et al., 2013, 2014) and in the Eastern Pontides (details in Topuz, 2002; Dokuz et al., 2006, 2010; Ustaömer et al., 2013). Upper Jurassic-Lower Cretaceous carbonates cover the Jurassic volcaniclastic sequence and the older rocks of the İstanbul and Sakarya zones (e.g., Pelin, 1977; Bergougnan, 1987; Tüysüz, 1999; Koch et al., 2008; Okay et al., 2017).

3. Jurassic volcanosedimentary sequence of the Eastern Pontides

The Jurassic volcanosedimentary sequence of the Eastern Pontides rests unconformably over the Upper Carboniferous sedimentary rocks in the Demirözü and Pulur regions (Bayburt) (Okay and Leven, 1996; Çapkınoğlu, 2003; Kandemir and Lerosey-Aubril, 2011) and over the Carboniferous crystalline basement, which is composed of metamorphic rocks and granitoids in Gümüşhane (Kandemir, 2004; Figures 1–3). The Jurassic volcanosedimentary sequence consists of a thick series of volcaniclastic sandstones with alternations of tuffs and Ammonitico Rosso type limestones in the Eastern Pontides (Pelin, 1977; Bergougnan, 1987; Kandemir, 2004). The Jurassic Şenköy Formation has a thickness of up to 2243 m and shows abrupt changes in thickness and facies along the basin (details in Kandemir, 2004). It starts with coal-bearing sandstone and conglomerate passing up into a thick volcanosedimentary sequence composed of lithic tuff, volcanogenic sandstone, and shale interbedded with basaltic and andesitic lavas. Ammonitico Rosso type condensate limestone levels locally occur in the lower parts of the Şenköy Formation with Sinemurian-Pliensbachian fossil assemblages of ammonites, brachiopods, bivalves,

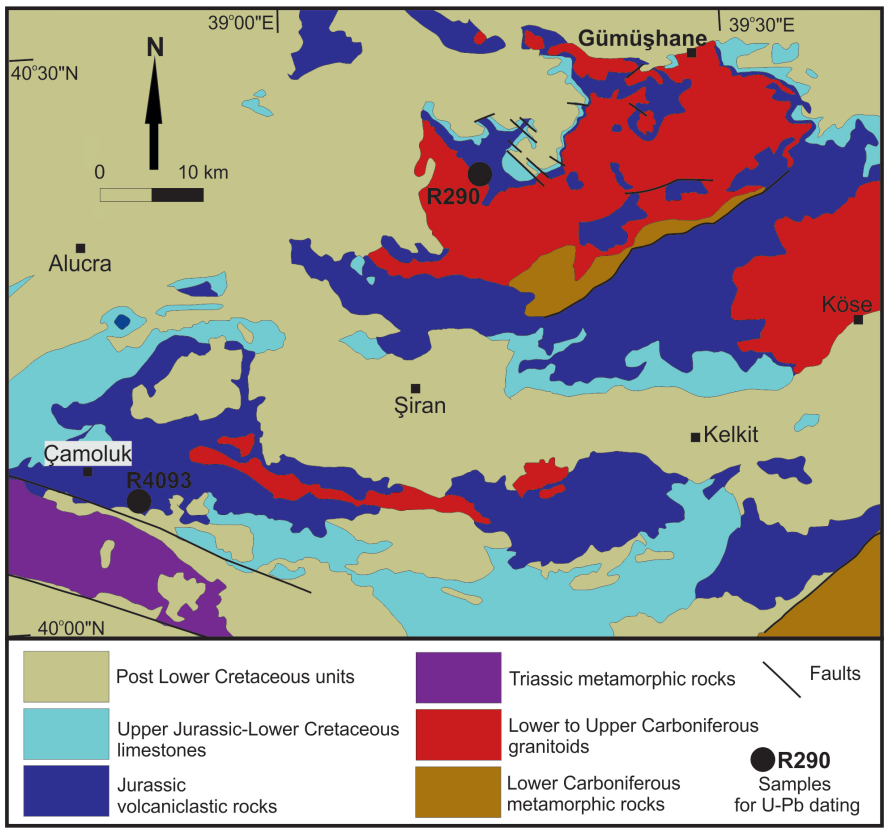

Figure 2. Geological map of the study area together with the locations of the dated samples (modified after Akdeniz and Güven, 2002; Hakyemez and Papak, 2002).

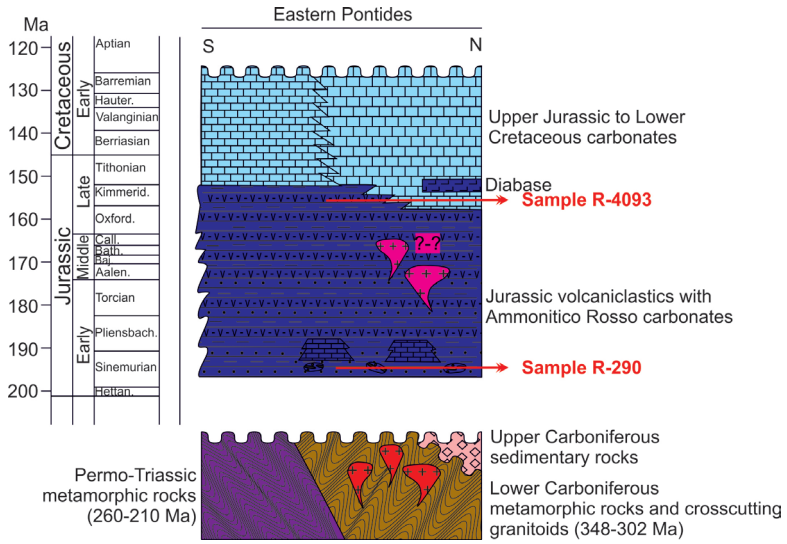

Figure 3. Generalized stratigraphic section of the Eastern Pontides for the pre-Cretaceous.

gastropods, belemnites, crinoids, and foraminifera (Alkaya and Meister, 1995; Kandemir and Yılmaz, 2009; Vörös and Kandemir, 2011). The upper levels of the Şenköy Formation are mainly represented by volcanics and volcaniclastic rocks that have not been dated.

The depositional environment of the Şenköy Formation ranges from paralic to marine (Robinson et al., 1995; Kandemir, 2004). An extensional tectonic regime is assigned to the Jurassic basin of the Eastern Pontides due to: i) rapid lateral changes in facies and thickness (Kandemir, 2004; Akdoğan, 2011); ii) hardgrounds within the sequence, which are cut by Neptunian dykes of red pelagic limestone of Ammonitico Rosso facies; iii) extensive submarine volcanism accompanying sedimentation; iv) the presence of synsedimentary normal faulting. The Jurassic magmatic/volcanic-volcaniclastic rocks are also widely exposed in the Central Pontides. The westernmost continuation of the Şenköy Formation is in the western part of the Sakarya Zone in the Mudurnu region (Altıner et al., 1991; Genç and Tüysüz, 2010). The geochemistry and isotopic data of the Jurassic volcanic/plutonic rocks from the Pontides, Crimea, and the Caucasus show typical features of subduction-related arc magmatism rather than that of rifting (Mengel et al., 1987; Boztuğ et al., 1995; Şen, 2007; Nzegge, 2008; Dokuz et al., 2010; Genç and Tüysüz, 2010; McCann et al., 2010; Meijers et al., 2010; Adamia et al., 2011; Okay et al., 2014). The Jurassic magmatic arc is assigned to the northward subduction of the İzmir-Ankara-Erzincan Ocean beneath the Pontides, which during the Jurassic was located on the southern margin of Laurasia (Çelik et al., 2011; Okay et al., 2013, 2014; Topuz et al., 2013; Okay and Nikishin, 2015).

4. U-Pb dating methods

Thin sections and mineral separation were done at İstanbul Technical University for U-Pb geochronology. Zircons were extracted from sandstone samples by using standard separation techniques including crushing, milling, sieving, and rinsing. The dried sand fractions were magnetically separated and heavy liquid was used to separate the heavy minerals. Special care was taken in order to achieve unbiased handpicking of zircons (e.g., regardless of size, shape, color, degree of rounding, and transparency). The crystals were embedded in an epoxy mount of 25 mm in diameter, lapped by 2500-mesh SiC paper, and polished by 9-, 3-, and 1-µm diamond suspensions. Cathodoluminescence (CL) images were obtained from zircons using a JEOL JXA 8900 electron microprobe at the Geozentrum Göttingen in order to study their internal structure and to select homogeneous parts for the in situ age determinations. The in situ U-Pb dating was performed by laser-ablation single-collector sector-field inductively coupled plasma mass spectrometry (LA-SF-ICP-MS). A Thermo Finnigan Element 2 mass spectrometer coupled to a Resonetics Excimer laser ablation system was used. All age data presented here were obtained by single spot analyses with a laser beam diameter of 33 µm and a crater depth of approximately 10 µm. Zircon grains were randomly selected for analysis. The laser was fired at a repetition rate of 5 Hz and at nominal laser energy output of 25%. The carrier gas was He and Ar. The age calculation and quality control are based on the drift and fractionation correction by standard-sample bracketing using GJ-1 zircon reference material (Jackson et al., 2004). For further control, the Plešovice zircon (Sláma et al., 2008) and the

91500 zircon (Wiedenbeck et al., 1995) were analyzed as 'secondary standards'. Drift and fractionation corrections and data reductions were performed with UranOS data reduction software (Dunkl et al., 2008). The age data shown in the figures and discussions are according to $^{207}Pb/^{206}Pb$ ages for grains older than 1.0 Ga, and $^{206}Pb/^{238}U$ ages for younger grains.

The discordance % was calculated according to the following formulas: (1 – [(207/235Udate) / (206Pb/238Udate)] × 100 when ages were <1.0 Ga and (1 – [(207/206Pb date) / (206Pb /238Udate)]) × 100 when ages were >1.0 Ga. Ages with discordance of >5% were excluded from the discussion. The concordia plots and age spectra were constructed by the help of Isoplot/Ex 3.0 (Ludwig, 2012) and AgeDisplay (Sircombe, 2004). The age components of the plots were also verified using PopShare (Dunkl and Székely, 2002) and DensityPlotter (Vermeesch, 2012).

5. Results

5.1. Petrographic descriptions of the dated samples

To constrain the provenance and the maximum depositional age of the volcanoclastic part of the Şenköy Formation of the Eastern Pontides, we obtained U-Pb detrital zircon ages from two sandstone samples (R-290 and R-4093) (for locations, see Figure 2–4). UTM coordinates of the samples and single-grain U-Pb detrital zircon dating results are shown in the Table.

Sample R-290 was taken from medium-grained yellowish sandstone representing the lower part of the formation, 15 m above the late Carboniferous Gümüşhane granite, southwest of the city of Gümüşhane (Figures 2 and 4). The sandstones are overlain by the Ammonitico Rosso type condensate limestone, which has a well-constrained late Sinemurian-Pliensbachian depositional age (details in Alkaya and Meister, 1995; Kandemir and Yılmaz, 2009; Vörös and Kandemir, 2011). The sample is a medium-grained sandstone consisting of lithic fragments, quartz, feldspar, and altered mafic minerals in the fine-grained matrix of clay/sericite and calcite (Figures 5a and 5b). The grain size of the sample varies between 0.2 and 0.4 mm. Rock fragments are the most abundant components, making up 65% of the bulk, and are composed mainly of limestone and fossil fragments, metamorphic rock fragments, basaltic/andesitic volcanic rock fragments, and a few chert grains. Feldspar constitutes 10% of the sandstone and is largely replaced by calcite and sericite. Angular monocrystalline quartz grains make up 10% of the sandstone with minor polycrystalline quartz (3%).

Sample R-4093 was taken from the upper level of the Şenköy Formation south of Alucra (Figures 2 and 4). The fine- to medium-grained, well-sorted volcaniclastic

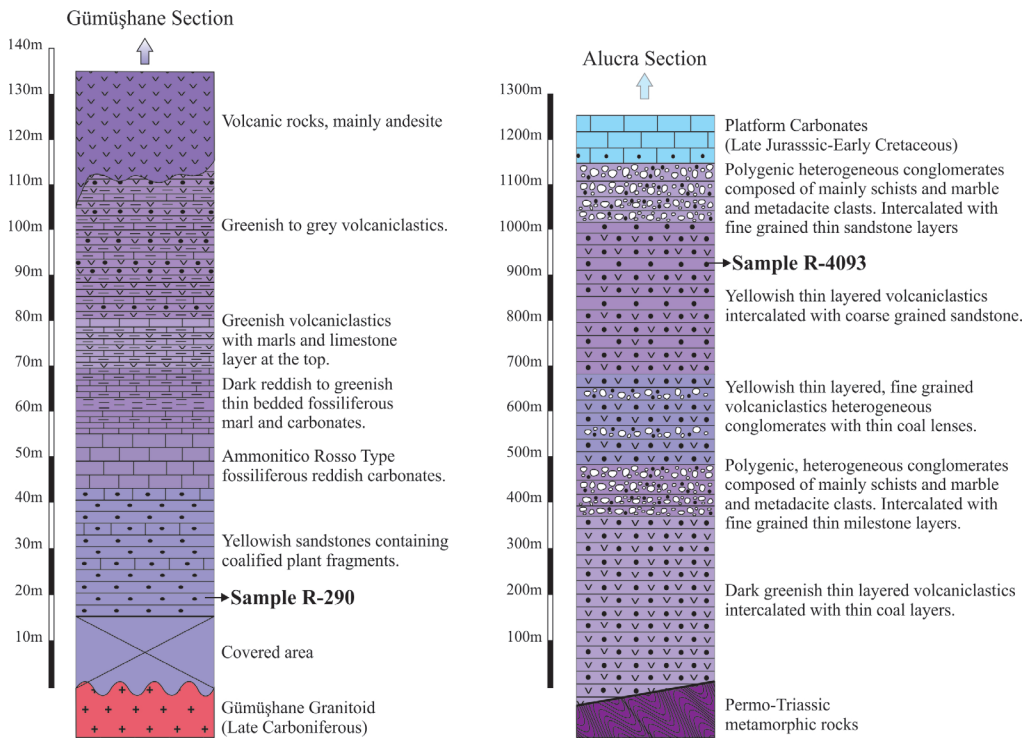

Figure 4. Local stratigraphic sections showing the approximate location of the samples (modified from Pelin, 1977; Kandemir, 2004).

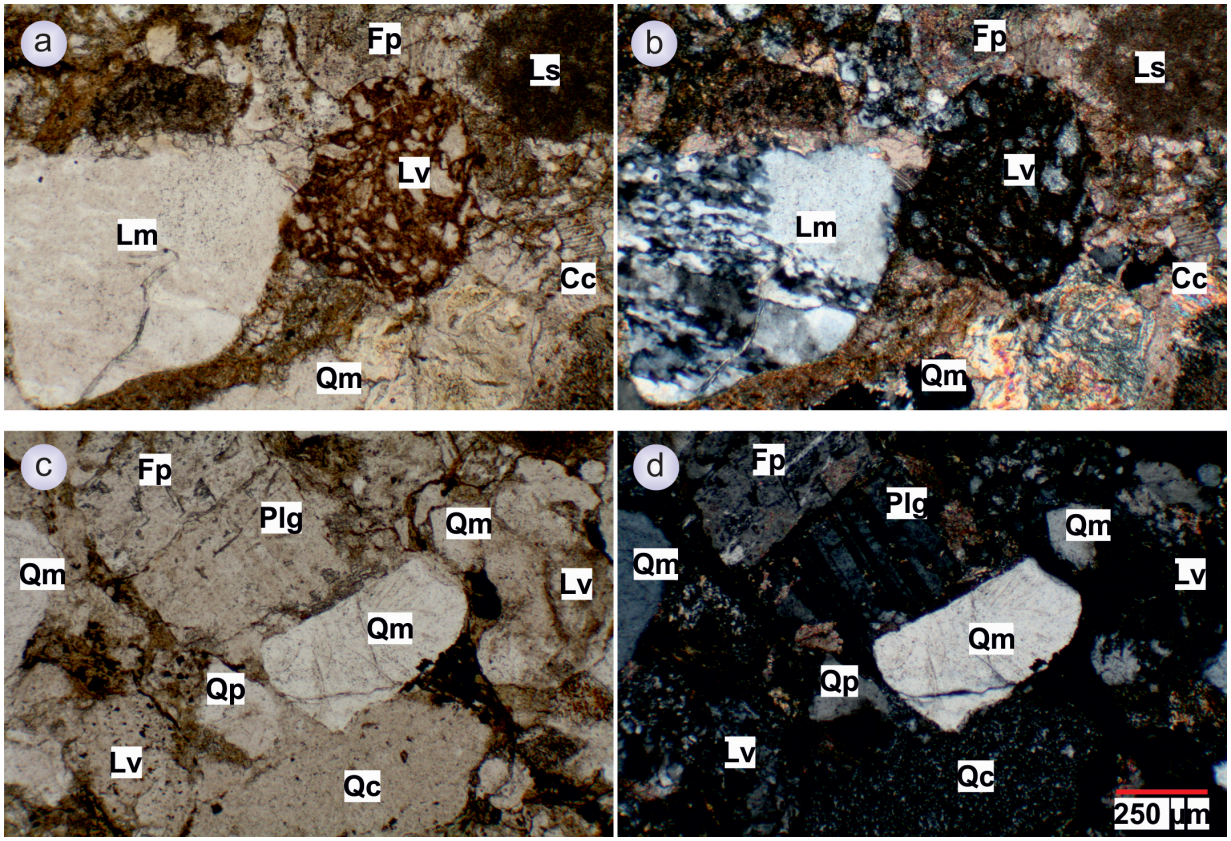

Figure 5. Photomicrographs of the analyzed Jurassic sandstones in plane-polarized light (left) and under crossed polarizers (right). a) and b) Sample R-290, c) and d) R-4093. Monocrystalline quartz (Qm), polycrystalline quartz (Qp), calcite (Cc), feldspar (Fp), plagioclase (Plg), metamorphic lithic fragment (Lm), volcanic rock fragment (Lv), limestone fragment (Ls), and chert (Qc).

sandstone is composed of feldspar (30%), rock fragments (35%), angular grains of quartz (25%), and muscovite (less than 1%), which are set in a matrix rich of sericite/clay and fine-grained calcite (10%) (Figures 5c and 5d). Angular nonaltered plagioclase grains showing albite twins make up 25% of the sample. Quartz grains, up to 0.7 mm in size, are composed mainly of monocrystalline grains (20%). Volcanic rock fragments are composed of fine-grained felsic and basaltic/andesitic rock fragments with well-oriented fine plagioclase laths. The metamorphic rock fragments are mainly composed of polycrystalline quartz. There are also angular to semirounded chert grains up to 0.5 mm in size (2%).

5.2. U-Pb ages of detrital zircons of the studied samples

In total 180 detrital zircon ages have been obtained from two samples of the Şenköy Formation, of which 154 (86%) are concordant at 95%–105% (Table). Concordia diagrams and CL images of the detrital zircon grains are given in Figures 6 and 7. The distribution of U-Pb ages from the two samples show three main age components at the Middle Jurassic (160–180 Ma; 27%, 41 grains), Late Triassic-Early Jurassic (190–210 Ma; 40%, 61 grains), and late Carboniferous (300–330 Ma; 14%, 22 grains) (Figure 8).

5.2.1. Sample R-290

Ninety-one single zircon grains from sample R-290 yielded 82 concordant (95%–105%) zircon ages with the youngest age of 184.7 ± 2.6 Ma (Early Jurassic, Pliensbachian) and the oldest age of 1954.5 ± 16.9 Ma (Paleoproterozoic) (Table). Most of the analyzed zircons from sample R-290 are remarkably euhedral and have clear oscillatory zonation in CL images, indicating a magmatic origin (Figure 7). The magmatic origin of the detrital zircons is also shown by the Th/U ratios of >0.1, which vary between 0.2 and 1.8 (Table; Figure 9). A few zircon grains show no zoning or patchy zoning (Figure 7). Of the detrital zircons, 67% (55 grains) yielded ages between 210 and 190 Ma (Rhaetian-Sinemurian) (Figure 10). There are few zircons scattered in the Triassic (7%, 6 grains), Paleozoic (12%, 10 grains), and Proterozoic (11%, 9 grains) without a significant peak.

5.2.2. Sample R-4093

Eighty-nine single zircon grains from sample R-4093 yielded 72 concordant (95%–105%) zircon ages with the

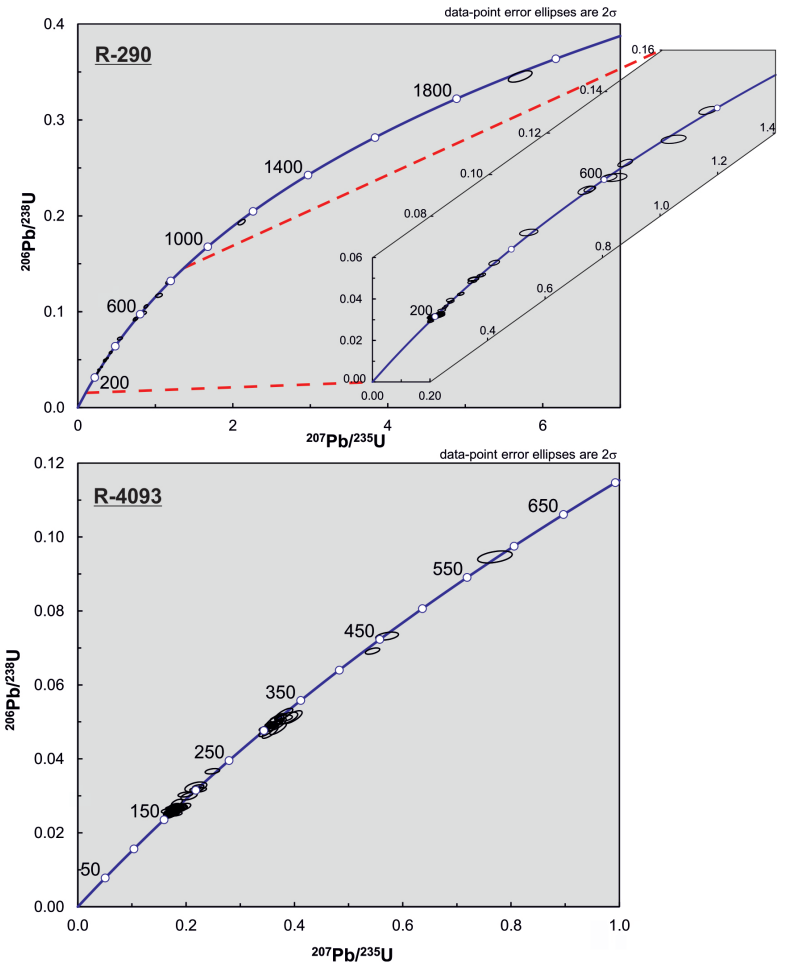

Figure 6. Concordia diagrams of the studied samples of the Şenköy Formation.

youngest age of 155.9 ± 1.8 Ma (Kimmeridgian) and the oldest age of 582.8 ± 7.8 Ma (Neoproterozoic) (Table; Figure 10). Most of the zircon grains are euhedral (Figure 7). The CL images of the dated zircon grains from sample R-4093 mostly exhibit a clear oscillatory zonation, indicating a magmatic origin (Figure 7). This is also supported by the Th/U values ranging between 0.18 and 1.58 (Table; Figure 9). The detrital age distribution pattern of sample R-4093 shows major populations at the Toarcian-Oxfordian (180–160 Ma; 57%, 41 grains) and late Carboniferous (330–300 Ma; 22%, 16 grains) (Figure 10). The other zircon grains yielded ages of Silurian (431.1 ± 4.5 Ma), Devonian (455.5 ± 5.5 Ma), and Neoproterozoic (582.8 ± 7.8 Ma).

6. Discussion and conclusions

6.1. The maximum depositional age of the Şenköy Formation

The depositional age of the Şenköy Formation is commonly regarded as Early-Middle Jurassic based on Sinemurian-Pliensbachian fossil assemblages of ammonites, brachiopods, bivalves, gastropods, belemnites, crinoids, and foraminifera from the Ammonitico Rosso type carbonate levels (Alkaya and Meister, 1995; Vörös and Kandemir, 2011), and Bathonian pollen and dinoflagellate assemblages detected in the clastic members (Robinson et al., 1995).

Studied samples R-4093 and R-290 yielded youngest ages of 155.9 ± 1.8 Ma (Late Jurassic, Oxfordian-Kimmeridgian) and 184.7 ± 2.6 Ma (Early Jurassic, Pliensbachian), respectively (Table; Figure 10). Considering the errors and the next youngest detrital zircon age, which is 158.0 ± 4.5 Ma (Table), the latest Oxfordian is most likely the maximum depositional age of the Şenköy Formation (according to the time table of Gradstein et al., 2012). This is compatible with the latest Oxfordian-Kimmeridgian age of the overlying carbonates of Berdiga Mountain (Koch et al., 2008). Thus, the depositional age of the Şenköy Formation extends from the Sinemurian to the latest Oxfordian for over 40 million years (Figures 3 and 10).

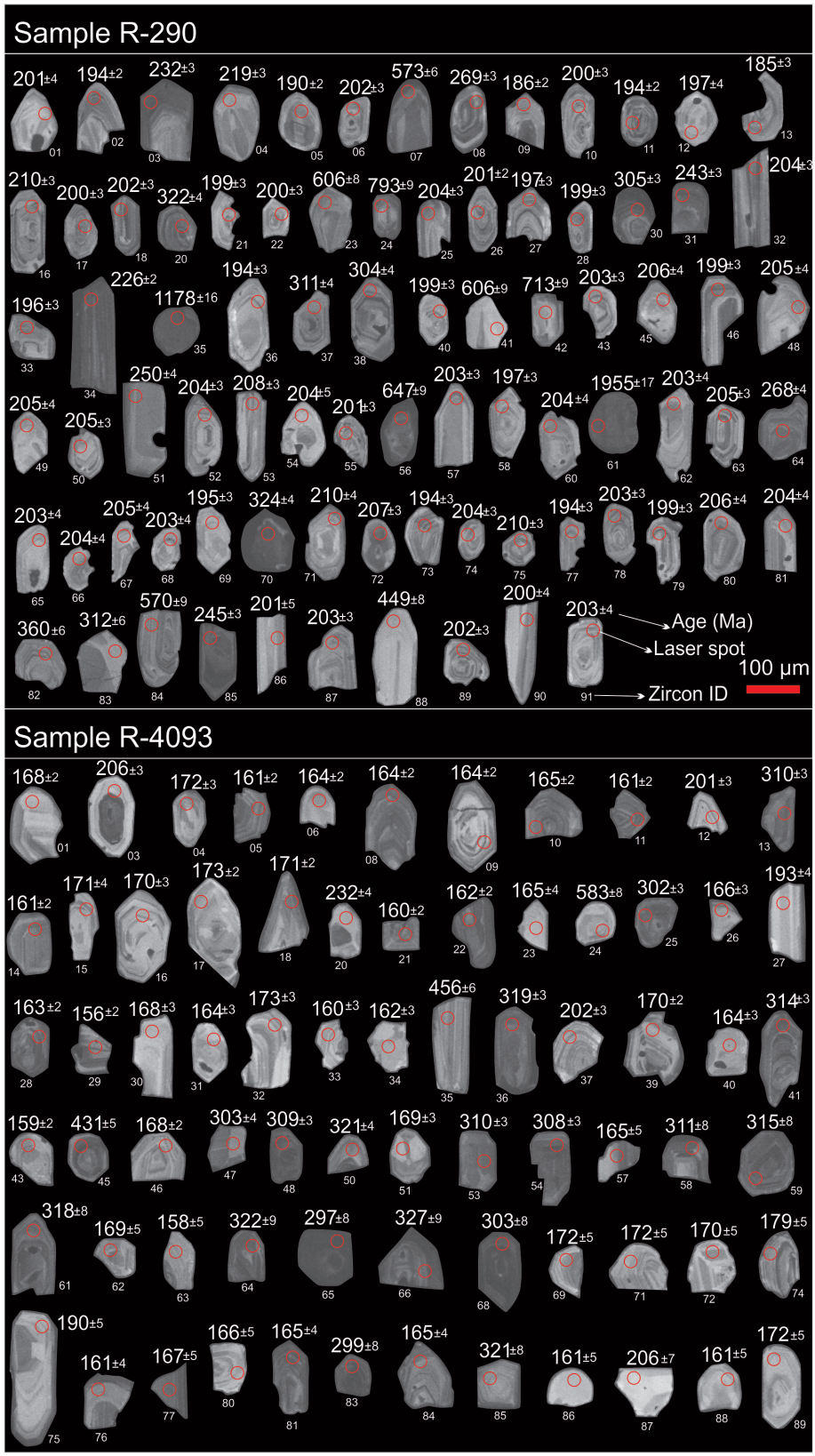

Figure 7. Cathodoluminescence images of the dated zircons from the two Jurassic sandstone samples. The laser ablation pits, marked by red circles, are 33 µm in diameter.

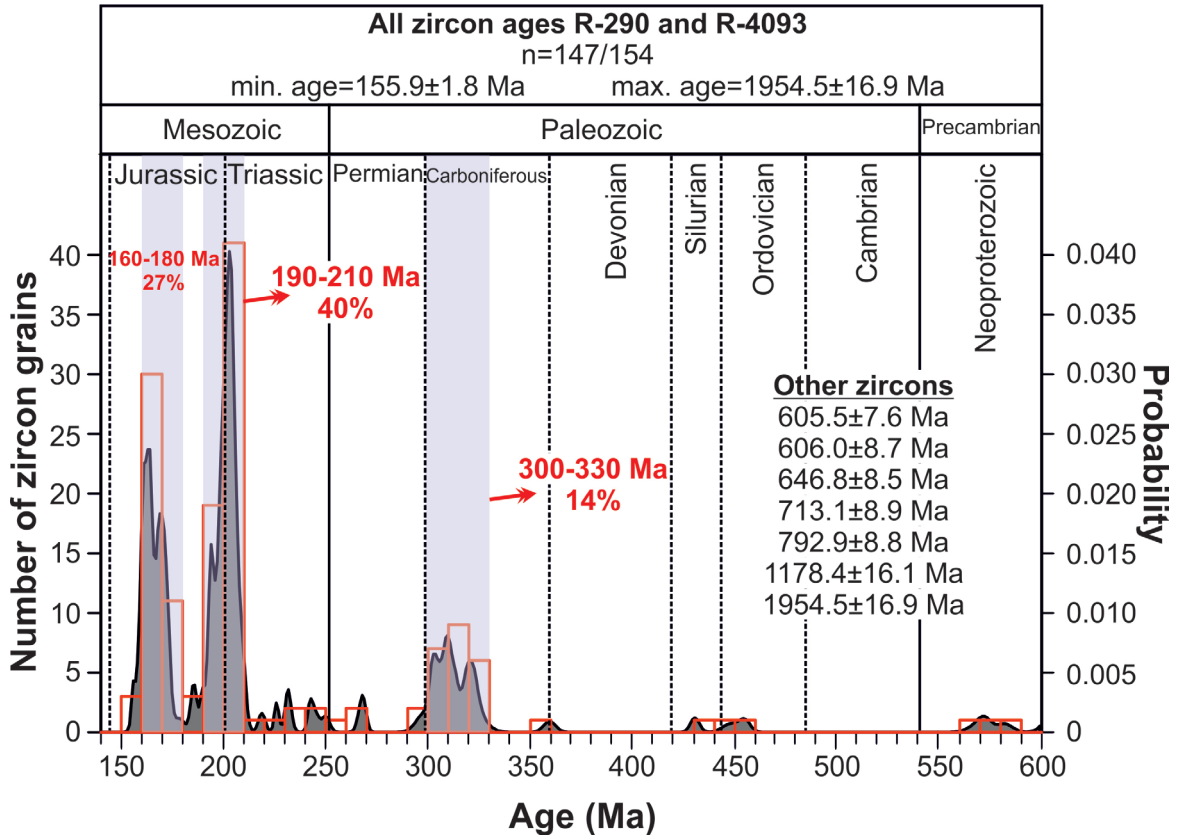

Figure 8. Histogram with probability density curves for all U-Pb detrital zircon ages obtained from studied samples of the Jurassic Şenköy Formation.

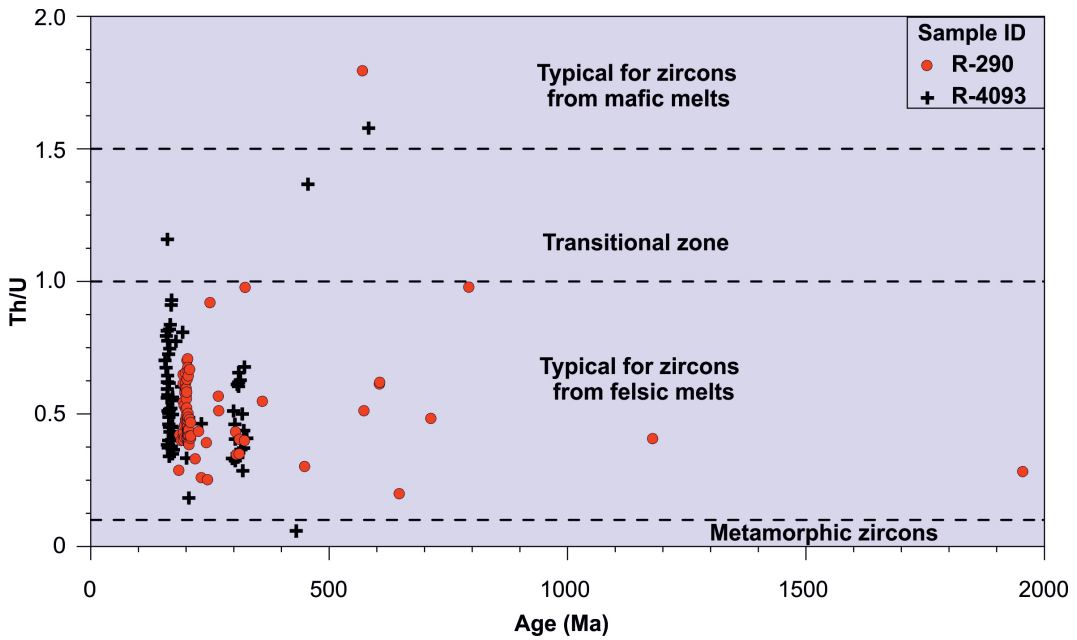

Figure 9. Th/U ratio versus U-Pb ages of the detrital zircons from two Jurassic sandstone samples. Discrimination lines are from Linnemann et al. (2011) and Rubatto (2002).

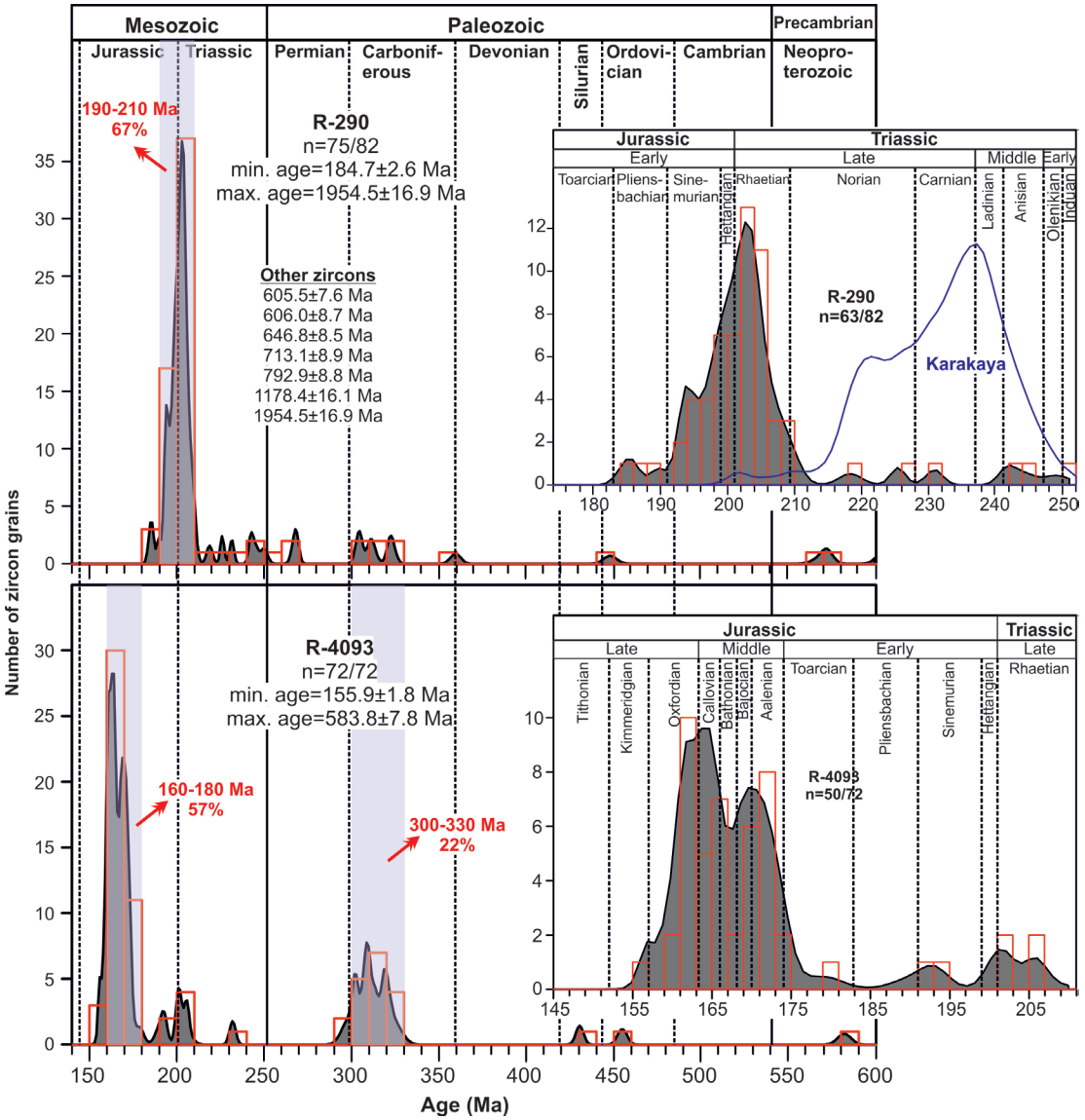

Figure 10. Histogram with probability density curves of U-Pb detrital zircon ages from two sandstone samples of the Jurassic Şenköy Formation. The blue probability density curve represents the Triassic U-Pb detrital zircon ages of the Karakaya Complex (Ustaömer et al., 2016).

6.2. Source of the Jurassic Şenköy Formation

The U-Pb detrital zircon distribution of the two samples show main populations at the Middle Jurassic (160–180 Ma; 27%, 41 grains) and Late Triassic-Early Jurassic (190–210 Ma; 39%, 61 grains), with a less dominant population of late Carboniferous (300–330 Ma; 14%, 22 grains) zircons (Figure 8). Detrital zircon distributions indicate two main magmatic sources for the Jurassic Şenköy Formation. One is the Jurassic arc magmatism, having a wide distribution in the Pontides and extending from Crimea through the Caucasus to Iran (e.g., Dokuz et al., 2006, 2010; Adamia et al., 2011; Okay et al., 2014; Okay and Nikishin, 2015), which was coeval with the deposition of the Early-Middle Jurassic Şenköy Formation (Figure 1). The other main source is the Late Triassic magmatism, marked by the distinct Late Triassic (Rhaetian; 203.4 ± 0.2 Ma) zircon age component in sample R-290 (Figures 8 and 10), which is taken from the lower part of the succession (Figures 2 and 4). However, the Triassic magmatic arc, related to Permo-Triassic subduction-accretionary complexes (Okay and Monié, 1997; Okay et al., 2002; Okay and Göncüoğlu, 2004; Topuz et al., 2004, 2014), are not known in the Eastern Pontides and are not exposed north of the Black Sea. Triassic detrital zircons are common in the Karakaya

Complex (Ustaömer et al., 2016) and in the Akgöl Flysch (Karslıoğlu et al., 2012; personal communication with T Ustaömer, 2017); however, the majority of the Triassic zircon ages cluster in the Ladinian to Norian (Figures 10 and 11). Such zircons (>210 Ma) are rare in the Şenköy Formation, making up only 5% (7 grains) of all dated zircons (Figures 8 and 10). This indicates little or no recycling from the Karakaya Complex or the Akgöl Flysch. Ustaömer et al. (2016) discussed the Triassic rocks of the Aegean Region, west of the Pontides, and revealed that they were not the source area of the Triassic detrital zircons of the Karakaya Complex. Long-distance derivation of zircons conflicts with the euhedral to subhedral crystal shapes of the Triassic zircons of the studied samples (Figure 7). The Th/U values of >0.1 (Figure 9), the internal structures, and the crystal shapes of the Triassic zircons support the idea that they were sourced from magmatic arc close to the basin, which is not exposed but may exist under the Jurassic-Neogene cover.

Late Carboniferous zircons (330–300 Ma), which make up only 14% (22 grains) of the studied samples, indicate a minor contribution from Carboniferous magmatic activity (Figure 8). Carboniferous granitoids (348–303 Ma) of the Eastern Pontides (e.g., Topuz et al., 2010; Dokuz, 2011; Kaygusuz et al., 2012, 2016; Figure 12) seem the most probable source for the late Carboniferous zircons. Significant contribution from synsedimentary magmatism (Figure 10) as illustrated with Sinemurian to Kimmeridgian zircons of the Şenköy Formation, which make up 42% of the detrital zircons, is generally attributed to arc flanking basins at convergent plate margins, like intra-arc basins (Cawood et al., 2012).

6.3. Triassic and Jurassic magmatism

The latest Triassic in the Sakarya Zone is marked by the Cimmeride orogeny ascribed to the collision and amalgamation of an oceanic edifice to the Laurasian margin. The Karakaya Complex related to this collision contains abundant Triassic zircons (Ustaömer et al., 2016) (Figures 10 and 11). However, a Triassic magmatic arc, related to the Late Triassic northward subduction, is not known from outcrops but is inferred to exist north of the Black Sea (Tikhomirov et al., 2004; Natal'in and Şengör,

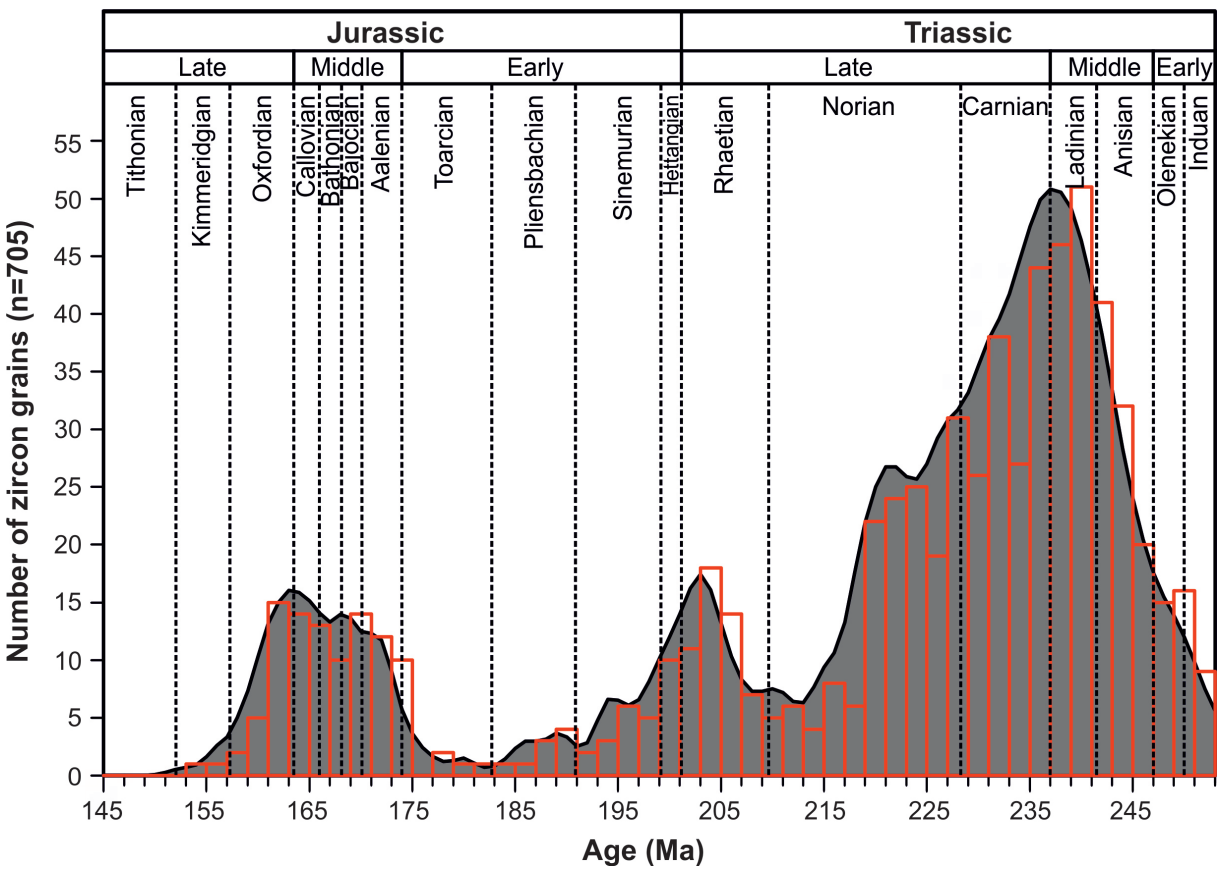

Figure 11. Histogram with probability density curves of Triassic and Jurassic U-Pb detrital zircon ages from the Jurassic Şenköy Formation (this study), the Karakaya Complex (from Ustaömer et al., 2016), the Lower Cretaceous sediments (Akdoğan et al., 2017), and Upper Cretaceous Flysch of the Central Pontides (our unpublished data).

Figure 12. Outcrops of pre-Jurassic rocks of the Black Sea region (modified from Okay and Nikishin, 2015, and references therein).

2005; Okay and Nikishin, 2015; Figure 12). Detrital zircon ages from studied samples in the Şenköy Formation show main populations at the Late Triassic-Early Jurassic (Rhaetian-Sinemurian; 210–190 Ma, 40%) and at latest the Early Jurassic-Late Jurassic (Toarcian-Oxfordian; 180–160 Ma, 27%) (Figures 8 and 10). These detrital zircons are mainly euhedral and have oscillatory zonation with Th/U values of >0.1 indicating felsic magmatic origin (Figures 7 and 9). The existence of Triassic and Jurassic magmatic zircons in the Jurassic samples together with those from the literature (Ustaömer et al., 2016; Akdoğan et al., 2017; our unpublished data) suggest that the arc magmatism extended from the Triassic into the Late Jurassic, possibly with a break in the Early Jurassic (187–175 Ma) (Figures 10 and 11).

Acknowledgments
This study was partly founded by TÜBA. We thank Gültekin Topuz for constructive comments, Raif Kandemir for his suggestions, Hayri Çolaker for help during field work, and Andreas Kronz (Göttingen) for kind help in the cathodoluminescence imaging of the zircon crystals.

References

Adamia S, Zakariadze G, Chkhotua T, Sadradze N, Tsereteli, N, Chabukiani A, Gventsadze A (2011). Geology of the Caucasus: a review. Turk J Earth Sci 20: 489-544.

Akdeniz N, Güven, IH (2002). Geological Map of Turkey, 1:500.000, Trabzon. Ankara, Turkey: General Directorate of Mineral Research and Exploration.

Akdoğan R, Okay AI, Sunal G, Tari G, Meinhold G, Kylander-Clark ARC (2017). Provenance of a large Lower Cretaceous turbidite submarine fan complex on the active Laurasian margin. J Asian Earth Sci 134: 309-329.

Alkaya F, Meister C, (1995). Liassic Ammonites from the central and eastern Pontides (Ankara and Kelkit areas, Turkey). Revue de Paléobiologie14: 125-193.

Altıner D, Koçyiğit A, Farinacci A, Nicosia U, Conti MA (1991). Jurassic–Lower Cretaceous stratigraphy and paleogeographic evolution of the southern part of north-western Anatolia (Turkey). Geologica Romana 27: 13-80.

Aysal N, Ustaömer T, Öngen S, Keskin M, Köksal S, Peytcheva I, Fanning M (2012). Origin of the Early-Middle Devonian magmatism in the Sakarya Zone, NW Turkey: Geochronology, geochemistry and isotope systematics. J Asian Earth Sci 45: 201-222.

Barrier E, Vrielynck B (2008). Atlas of Paleotectonic Maps of the Middle East (MEBE Program). Atlas of 14 Maps (Tectono–Sedimentary–Palinspastic maps from Late Norian to Pliocene), 1:18 500 000 scale. Paris, France: Univesité Pierre et Marie Curie.

Bergougnan H (1987). Etudes geologiques dans l'Est Anatolien. PhD, Univesité Pierre et Marie Curie, Paris, France.

Boztuğ D, Debon F, Le Fort P, Yılmaz O (1995). High compositional diversity of the Middle Jurassic Kastamonu Plutonic Belt, northern Anatolia, Turkey. Turk J Earth Sci 4: 67-86.

Çapkınoğlu Ş (2003). First records of conodonts from "the Permo-Carboniferous of Demirözü (Bayburt)", Eastern Pontides, NE Turkey. Turk J Earth Sci 12: 199-207.

Cawood PA, Hawkesworth CJ, Dhuime B, (2012). Detrital zircon record and tectonic setting. Geology 40: 875-878.

Çelik ÖF, Marzoli A, Marschik R, Chiaradia M, Neubauer F, Öz İ (2011). Early–Middle Jurassic intra-oceanic subduction in the İzmir-Ankara-Erzincan Ocean, Northern Turkey. Tectonophysics 509: 120-134.

Dercourt J, Ricou LE, Vrielynck B, editors (1993). Atlas Tethys Palaeoenvironmental Maps. Paris, France: Gauthier-Villars, Paris.

Dercourt J, Zonenshain LP, Ricou LE, Le Pichon X, Knipper AL, Grandjaquet C, Sbortshikov IM, Geussant J, Lepvrier C, Pechersku DH et al. (1986). Geological evolution of the Tethys belt from the Atlantic to the Pamirs since the Lias. Tectonophysics 123: 241-315.

Dokuz A (2011). A slab detachment and delamination model for the generation of Carboniferous high potassium I-type magmatism in the Eastern Pontides, NE Turkey: Köse composite pluton. Gondwana Res 19: 926-944.

Dokuz A, Karslı O, Chen B, Uysal I (2010). Sources and petrogenesis of Jurassic granitoids in the Yusufeli area, Northeastern Turkey: implications for pre- and post-collisional lithospheric thinning of the eastern Pontides. Tectonophysics 480: 258-279.

Dokuz A, Tanyolu E (2006). Geochemical constraints on the provenance, mineral sorting and subaerial weathering of Lower Jurassic and Upper Cretaceous clastic rocks of the Eastern Pontides, Yusufeli (Artvin), NE Turkey. Turk J Earth Sci 15: 181-209.

Dokuz A, Tanyolu E, Genç S (2006). A mantle-and a lower crust-derived bimodal suite in the Yusufeli (Artvin) area, NE Turkey: trace element and REE evidence for subduction-related rift origin of Early Jurassic Demirkent intrusive complex. Int J Earth Sci 95: 370-394.

Dunkl I, Mikes T, Simon K, von Eynatten H (2008). Brief introduction to the Windows program Pepita: data visualization, and reduction, outlier rejection, calculation of trace element ratios and concentrations from LA-ICP-MS data. In: Sylvester P, editor. Laser Ablation ICP-MS in the Earth Sciences: Current Practices and Outstanding Issues. Quebec City, Canada: Mineralogical Association of Canada, pp. 334-340.

Dunkl I, Székely B (2002). Component analysis with visualization of fitting–PopShare, a Windows program for data analysis. Geochim Cosmochim Ac 66: 201.

Genç SC, Tüysüz O (2010). Tectonic setting of the Jurassic bimodal magmatism in the Sakarya Zone (Central and Western Pontides), Northern Turkey: a geochemical and isotopic approach. Lithos 118: 95-111.

Gradstein FM, Ogg JG, Schmitz MD, Ogg GM (2012). The Geologic Time Scale 2012. Boston, MA, USA: Elsevier.

Hakyemez HY, Papak I (2002). Geological Map of Turkey, 1:500,000, Samsun. Ankara, Turkey: General Directorate of Mineral Research and Exploration.

Kandemir R (2004). Sedimentary characteristics and depositional conditions of Lower-Middle Jurassic Şenköy Formation in and around Gümüşhane. PhD, Karadeniz Technical University, Trabzon, Turkey.

Kandemir R, Lerosey-Aubril R (2011). First report of a trilobite in the Carboniferous of Eastern Pontides, NE Turkey. Turk J Earth Sci 20: 179-183.

Kandemir R, Yılmaz C (2009). Lithostratigraphy, facies, and deposition environment of the lower Jurassic Ammonitico Rosso type sediments (ARTS) in the Gümüşhane area, NE Turkey: implications for the opening of the northern branch of the Neo-Tethys Ocean. J Asian Earth Sci 34: 586-598.

Karslıoğlu Ö, Ustaömer T, Robertson AHF, Peytcheva I (2012). Age and provenance of detrital zircons from a sandstone turbidite of the Triassic-Early Jurassic Küre Complex, Central Pontides. In: Abstracts of the International Earth Science Colloquium on the Aegean Region, p. 57.

Kaygusuz A, Arslan M, Siebel W, Sipahi F, İlbeyli N (2012). Geochronological evidence and tectonic significance of Carboniferous magmatism in the southwest Trabzon area, eastern Pontides, Turkey. Int Geol Rev 54: 1776-1800.

Kaygusuz A, Arslan M, Sipahi F, Temizel İ (2016). U–Pb zircon chronology and petrogenesis of Carboniferous plutons in the northern part of the Eastern Pontides, NE Turkey: constraints for Paleozoic magmatism and geodynamic evolution. Gondwana Res 39: 327-346.

Koch R, Bucur II, Kırmacı MZ, Eren M, Taslı K (2008). Upper Jurassic and Lower Cretaceous carbonate rocks of the Berdiga Limestone–Sedimentation on an onbound platform with volcanic and episodic siliciclastic influx. Biostratigraphy, facies and diagenesis (Kircaova, Kale-Gümüşhane area; NE-Turkey). Neues Jahrb Geol P-A 247: 23-61.

Linnemann U, Ouzegane K, Drareni A, Hofmann M, Becker S, Gärtner A, Sagawe A (2011). Sands of West Gondwana: An archive of secular magmatism and plate interactions–A case study from the Cambro–Ordovician section of the Tassili Ouan Ahaggar (Algerian Sahara) using U–Pb-LA–ICP-MS detrital zircon ages. Lithos 123: 188-203.

Ludwig KR (2012). User's Manual for Isoplot 3.75: A Geochronological Toolkit for Microsoft Excel. Berkeley, CA, USA: Berkeley Geochronology Center.

McCann T, Chalot-Prat F, Saintot A (2010). The Early Mesozoic evolution of the Western Greater Caucasus (Russia): Triassic-Jurassic sedimentary and magmatic history. Geol Soc Spec Publ 340: 181-238.

Meijers MJM, Vrouwe B, Van Hinsbergen DJJ, Kuiper KF, Wijbrans J, Davies GR, Stephenson RA, Kaymakçı N, Matenco L, Saintot A (2010). Jurassic arc volcanism on Crimea (Ukraine): implications for the paleo-subduction zone configuration of the Black Sea region. Lithos 119: 412-426.

Mengel K, Borsuk AM, Gurbanov AG, Wedepohl KH, Baumann A, Hoefs J (1987). Origin of spilitic rocks from the southern slope of the Greater Caucasus. Lithos 20: 115-133.

Natal'in BA, Şengör AMC (2005). Late Palaeozoic to Triassic evolution of the Turan and Scythian platforms: The pre-history of the Palaeo-Tethyan closure. Tectonophysics 404: 175-202.

Nzegge OM (2008). Petrogenesis and geochronology of the Deliklitaş, Sivrikaya and Devrekani granitoids and basement, Kastamonu belt–Central Pontides (NW Turkey): Evidence for Late Palaeozoic-Mesozoic plutonism and geodynamic interpretation. PhD, University of Tübingen, Tübingen, Germany.

Nzegge OM, Satır M, Siebel W, Taubald H (2006). Geochemical and isotopic constraints on the genesis of the Late Palaeozoic Deliktaş¸ and Sivrikaya granites from the Kastamonu granitoid belt (Central Pontides, Turkey). Neues JB Miner Abh 183: 27-40.

Okay AI (1996). Granulite facies gneisses from the Pulur region, Eastern Pontides. Turk J Earth Sci 5: 55-61.

Okay AI, Altıner D, Sunal G, Aygül M, Akdoğan R, Altıner S, Simmons M (2017). Geological evolution of the Central Pontides. Geol Soc Spec Publ (in press).

Okay AI, Göncüoğlu MC (2004). Karakaya Complex: a review of data and concepts. Turk J Earth Sci 13: 77-95.

Okay AI, Gürsel S, Sherlock S, Altıner D, Tüysüz O, Kylander-Clark ARC, Aygül M (2013). Early Cretaceous sedimentation and orogeny on the active margin of Eurasia; Southern Central Pontides, Turkey. Tectonics 32: 1247-1271.

Okay AI, Gürsel S, Tüysüz O, Sherlock S, Keskin M, Kylander-Clark ARC (2014). Low-pressure - high-temperature metamorphism during extension in a Jurassic magmatic arc, Central Pontides, Turkey. J Metamorph Geol 32: 49-69.

Okay AI, Leven EJ (1996). Stratigraphy and paleontology of the Upper Paleozoic sequences in the Pulur (Bayburt) region, Eastern Pontides. Turk J Earth Sci 5: 145-155.

Okay AI, Monié P (1997). Early Mesozoic subduction in the Eastern Mediterranean: Evidence from Triassic eclogite in the northwest Turkey. Geology 25: 595-598.

Okay AI, Monod O, Monié P (2002). Triassic blueschists and eclogites from northwest Turkey: vestiges of the Paleo-Tethyan subduction. Lithos 64: 155-178.

Okay AI, Nikishin AM (2015). Tectonic evolution of the southern margin of Laurasia in the Black Sea region. Int Geol Rev 57: 1051-1076.

Okay AI, Şahintürk Ö (1997). Geology of the Eastern Pontides. In: Robinson AG, editor. Regional and Petroleum Geology of the Black Sea and Surrounding Region. AAPG Memoir 68. Tulsa, OK, USA: AAPG, pp. 291-311.

Okay AI, Satır M, Maluski H, Siyako M, Monié P, Metzger R, Akyüz S (1996). Paleo- and Neo-Tethyan events in northwest Turkey: geological and geochronological constraints. In: Yin A, Harrison M, editors. Tectonics of Asia. Cambridge, UK: Cambridge University Press, pp. 420-441.

Okay AI, Satır M, Siebel W (2006a). Pre-Alpide orogenic events in the Eastern Mediterranean region, European Lithosphere Dynamics. Geol Soc Mem 32: 389-405.

Okay AI, Tüysüz O (1999). Tethyan sutures of northern Turkey. Geol Soc Spec Publ 156: 475-515.

Okay AI, Tüysüz O, Satır M, Özkan-Altıner S, Altıner D, Sherlock S, Eren RH (2006b). Cretaceous and Triassic subduction-accretion, high-pressure-low-temperature metamorphism, and continental growth in the Central Pontides, Turkey. Geol Soc Am Bull 118: 1247-1269.

Pelin S (1977). Alucra (Giresun) Güneydogu Yöresinin Petrol Olanaklarl Bakımından Jeolojik İncelenmesi. Trabzon, Turkey: Karadeniz Technical University (in Turkish).

Robertson AHF, Dixon JE (1984). Introduction: aspects of the geological evolution of the Eastern Mediterranean. Geol Soc Spec Publ 17: 1-74.

Robinson AG, Banks CJ, Rutherford MM, Hirst JPP (1995). Stratigraphic and structural development of the Eastern Pontides, Turkey. J Geol Soc 152: 861-872.

Rubatto D (2002). Zircon trace element geochemistry: partitioning with garnet and the link between U–Pb ages and metamorphism. Chem Geol 184: 123-138.

Şen C (2007). Jurassic volcanism in the Eastern Pontides: Is it rift related or subduction related? Turk J Earth Sci 16: 523-539.

Şengör AMC (1984). The Cimmeride orogenic system and the tectonics of Eurasia. Geol Soc Am Spec Publ 195: 1-74.

Sircombe KN (2004). AgeDisplay: an EXCEL workbook to evaluate and display univariate geochronological data using binned frequency histograms and probability density distributions. Comput Geosci 30: 21-31.

Sláma J, Košler J, Condon DJ, Crowley JL, Gerdes A, Hanchar JM, Horstwood MSA, Morris GA, Nasdala L, Norberg N et al. (2008). Plešovice zircon - A new natural reference material for U-Pb and Hf isotopic microanalysis. Chem Geol 249: 1-35.

Stampfli GM, Borel GD (2002). A plate tectonic model for the Paleozoic and Mesozoic constrained by dynamic plate boundaries and restored synthetic oceanic isochrons. Earth Planet Sci Lett 196: 17-33.

Sunal G (2012). Devonian magmatism in the western Sakarya Zone, Karacabey Region, NW Turkey. Geodin Acta 25: 183-201.

Tikhomirov PL, Chalot-Prat F, Nazarevich BP (2004). Triassic volcanism in the Eastern Fore-Caucasus: evolution and geodynamic interpretation. Tectonophysics 381: 119-142.

Topuz G (2002). Petrology of mafic to ultramafic intrusions from the Pulur Massif, Eastern Pontides, NE Turkey. In: Proceedings of the 1st International Symposium of the Faculty of Mines (İTU) on Earth Sciences and Engineering, İstanbul, p. 129.

Topuz G, Altherr R, Kalt A, Satır M, Werner O, Schwarz WH (2004). Aluminous granulites from the Pulur complex, NE Turkey: a case of partial melting, efficient melt extraction and crystallization. Lithos 72: 183-207.

Topuz G, Altherr R, Schwarz WH, Dokuz A, Meyer HP (2007). Variscan amphibolite facies metamorphic rocks from the Kurtoğlu metamorphic complex (Gümüşhane area, Eastern Pontides, Turkey). Int J Earth Sci 96: 861-873.

Topuz G, Altherr R, Siebel W, Schwarz WH, Zack T, Hasözbek A, Barth M, Satır M, Şen C (2010). Carboniferous high-potassium I-type granitoid magmatism in the Eastern Pontides: the Gümüşhane pluton (NE Turkey). Lithos 116: 92-110.

Topuz G, Göçmengil G, Rolland Y, Çelik ÖF, Zack T, Schmitt AK (2013). Jurassic accretionary complex and ophiolite from northeast Turkey: no evidence for the Cimmerian continental ribbon. Geology 41: 255-258.

Topuz G, Okay AI, Altherr R, Schwarz WH, Sunal G, Altınkaynak L (2014). Triassic warm subduction in northeast Turkey: evidence from the Ağvanis metamorphic rocks. Isl Arc 23: 181-205.

Tüysüz O (1999). Geology of the Cretaceous sedimentary basins of the Western Pontides. Geol J 34: 75-93.

Ustaömer PA, Ustaömer T, Robertson AHF (2012). Ion probe U-Pb dating of the central Sakarya basement: a peri-Gondwana terrane intruded by late lower Carboniferous subduction/collision-related granitic rocks. Turk J Earth Sci 21: 905-932.

Ustaömer T, Robertson AHF (1993). A Late Palaeozoic-Early Mesozoic marginal basin along the actives sourthern continental margin of Eurasia: evidence from the central Pontides (Turkey) and adjacent regions: Geol J 28: 219-238.

Ustaömer T, Robertson AHF (1994). Late Palaezoic marginal basin and subduction-accretion: the Palaeotethyan Küre Complex, Central Pontides, northern Turkey. J Geol Soc London 151: 291-305.

Ustaömer T, Robertson AHF (1997). Tectonic-sedimentary evolution of the north Tethyan margin in the Central Pontides of northern Turkey. In: Robinson AG, editor. Regional and Petroleum Geology of the Black Sea and Surrounding Region. American Association of Petroleum Geologists Memoir 68. Tulsa, OK, USA: AAPG, pp. 255-290.

Ustaömer T, Robertson AHF, Ustaömer PA, Gerdes A, Peytcheva I (2013). Constraints on Variscan and Cimmerian magmatism and metamorphism in the Pontides (Yusufeli–Artvin area), NE Turkey from U-Pb dating and granite geochemistry. Geol Soc Spec Publ 372: 49-74.

Ustaömer T, Ustaömer PA, Robertson AHF, Gerdes A (2016). Implications of U–Pb and Lu–Hf isotopic analysis of detrital zircons for the depositional age, provenance and tectonic setting of the Permian–Triassic Palaeotethyan Karakaya Complex, NW Turkey. Int J Earth Sci 105: 7-38.

Vermeesch P (2012). On the visualisation of detrital age distributions. Chemical Geol 312: 190-194.

Vörös A, Kandemir R (2011). A new Early Jurassic brachiopod fauna from the Eastern Pontides (Turkey). Neues Jahrb Geol P-A 260: 343-363.

Wedding H (1963). Beiträge zur Geologie der Kelkitlinie und zur Stratigraphie des Jura im Gebiet Kelkit-Bayburt (Gümüşhane). Bulletin of the Mineral Research and Exploration Institute of Turkey 61: 31-37 (in German).

Wiedenbeck M, Allé P, Corfu F, Griffin WL, Meier M, Oberli F, von Quadt A, Roddick JC, Spiegel W (1995). Three natural zircon standards for U–Th–Pb, Lu–Hf, trace element and REE analyses. Geostandard Newslett 19: 1-23.

Yılmaz O, Boztuğ D (1986). Kastamonu granitoid belt of northern Turkey: first arc plutonism product related to the subduction of the Paleo-Tethys. Geology 14: 179-183.

Table. U-Pb isotopic data on the analyzed zircons.

				Isotopic ratios								Ages (Ma)									
	U	Th	Pb	^{208}Pb	^{206}Pb	±1s	^{207}Pb	±1s	^{207}Pb	±1s	rho	^{206}Pb	±2s	^{207}Pb	±2s	^{207}Pb	±2s	Best age*	±2s	Conc**	Discord#
	[ppm]	U	[ppm]	^{206}Pb	^{238}U	[%]	^{235}U	[%]	^{206}Pb	[%]		^{238}U	[Ma]	^{235}U	[Ma]	^{206}Pb	[Ma]	(Ma)	[Ma]	(%)	(%)
Sample_R-290 (UTM: 37T 0518537E, 4469064N)																					
1	83	0.449	34	0.155	0.032	1.1	0.222	3.9	0.051	3.7	0.28	200.9	4.3	203.5	14.3	234.1	85.9	200.9	4.3	99	–1
2	482	0.675	296	0.233	0.031	0.6	0.212	1.4	0.050	1.3	0.4	193.9	2.1	195.6	4.9	216.5	29.6	193.9	2.1	99	–1
3	929	0.285	241	0.100	0.037	0.6	0.256	1.1	0.051	1	0.48	231.6	2.5	231.3	4.8	228.4	23.6	231.6	2.5	100	0
4	130	0.362	43	0.124	0.035	0.8	0.241	2.3	0.051	2.2	0.34	218.9	3.4	219.1	9.2	221.5	51.1	218.9	3.4	100	0
5	280	0.438	112	0.154	0.030	0.7	0.201	1.6	0.049	1.5	0.41	189.8	2.4	185.7	5.4	134.8	34.5	189.8	2.4	102	2
6	221	0.493	100	0.180	0.032	0.8	0.233	2.1	0.053	1.9	0.36	202.3	3	212.3	8	324.5	44.2	202.3	3.0	95	–5
7	293	0.566	150	0.224	0.093	0.6	0.756	1.1	0.059	1	0.51	573	6.3	571.7	9.8	566.6	21.3	573.0	6.3	100	0
8	535	0.562	274	0.192	0.043	0.6	0.310	1.1	0.053	1	0.5	268.5	3	274.5	5.5	325.5	23	268.5	3.0	98	–2
9	233	0.464	98	0.155	0.029	0.6	0.204	1.8	0.051	1.7	0.35	186	2.3	188.3	6.3	217.9	39.8	186.0	2.3	99	–1
10	307	0.625	175	0.210	0.032	0.6	0.219	1.7	0.050	1.6	0.37	199.9	2.5	201.3	6.2	217.7	37.1	199.9	2.5	99	–1
11	679	0.712	440	0.248	0.030	0.5	0.216	1.3	0.051	1.2	0.4	193.7	2	198.4	4.8	255.3	28.4	193.7	2.0	98	–2
12	78	0.451	32	0.164	0.031	0.9	0.208	3.5	0.049	3.4	0.27	197.1	3.7	191.6	12.4	125	80.2	197.1	3.7	103	3
13	212	0.315	61	0.108	0.029	0.7	0.200	1.8	0.050	1.7	0.39	184.7	2.6	185.3	6.2	192.6	39.2	184.7	2.6	100	0
14	364	0.371	123	0.170	0.035	0.6	0.324	1.5	0.067	1.4	0.4	221.8	2.6	285.3	7.5	844.2	29.2	221.8	2.6	78	–29
15	162	0.589	87	0.198	0.320	0.5	5.994	0.9	0.136	0.7	0.61	1788	17.1	1975	15.5	2176.5	13.8	2176.5	13.8	82	–22
16	168	0.456	70	0.158	0.033	0.7	0.233	1.9	0.051	1.8	0.38	209.6	3.1	212.4	7.5	244.4	41.7	209.6	3.1	99	–1
17	250	0.541	123	0.190	0.032	0.7	0.218	1.8	0.050	1.6	0.39	200.4	2.7	199.9	6.4	193.7	37.9	200.4	2.7	100	0
18	509	0.657	321	0.236	0.032	0.8	0.219	1.5	0.050	1.3	0.52	202	3.1	200.9	5.4	187.6	29.9	202.0	3.1	101	1
19	209	0.583	111	0.213	0.031	0.7	0.242	1.6	0.056	1.5	0.43	199.6	2.7	220.3	6.5	447.2	33.3	199.6	2.7	91	–10
20	378	0.438	151	0.153	0.051	0.6	0.375	1.2	0.053	1.1	0.47	322.2	3.7	323	6.9	328.9	25.2	322.2	3.7	100	0
21	141	0.568	73	0.190	0.031	0.7	0.220	2.3	0.051	2.2	0.31	199.3	2.8	201.9	8.3	231.6	50	199.3	2.8	99	–1
22	143	0.528	69	0.180	0.031	0.7	0.220	2.2	0.051	2.1	0.3	199.8	2.7	201.6	8.2	223.5	49.3	199.8	2.7	99	–1
23	106	0.676	65	0.229	0.098	0.7	0.822	1.4	0.061	1.3	0.46	605.5	7.6	609.2	13.1	623.1	27.6	605.5	7.6	99	–1
24	185	1.083	181	0.345	0.131	0.6	1.166	1.1	0.065	0.9	0.53	792.9	8.8	785	12.2	762.6	20.5	792.9	8.8	101	1
25	275	0.555	138	0.188	0.032	0.6	0.217	1.4	0.049	1.2	0.46	204	2.5	199	4.9	140.4	28.8	204.0	2.5	103	2
26	383	0.641	223	0.229	0.032	0.6	0.218	1.4	0.050	1.2	0.44	201.2	2.4	200.4	5	191.2	29	201.2	2.4	100	0
27	260	0.638	151	0.212	0.031	0.6	0.216	1.7	0.050	1.6	0.38	197.2	2.5	198.5	6.1	213.8	36.5	197.2	2.5	99	–1

Table. (Continued).

28	296	0.518	141	0.186	0.031	0.6	0.216	1.8	0.050	1.7	0.35	198.6	2.5	198.4	6.4	196.5	38.8	198.6	2.5	100	0
29	99	0.48	43	0.170	0.030	0.9	0.233	2.6	0.055	2.5	0.35	193.1	3.5	212.3	10.1	430.9	55.3	193.1	3.5	91	−10
30	1060	0.38	368	0.131	0.049	0.5	0.354	1	0.053	0.8	0.54	305.3	3.1	307.7	5.2	326.3	19.3	305.3	3.1	99	−1
31	554	0.43	217	0.151	0.038	0.5	0.270	1.2	0.051	1.1	0.43	242.5	2.5	242.5	5.2	242.8	25.4	242.5	2.5	100	0
32	258	0.53	126	0.190	0.032	0.7	0.227	1.8	0.051	1.7	0.36	203.6	2.6	207.8	6.8	255.3	38.8	203.6	2.6	98	−2
33	307	0.584	163	0.198	0.031	0.7	0.210	1.5	0.049	1.3	0.45	196	2.6	193.5	5.2	163.7	31.3	196.0	2.6	101	1
34	739	0.476	321	0.166	0.036	0.5	0.250	1.2	0.051	1.1	0.43	226.1	2.2	226.7	4.8	232.9	25	226.1	2.2	100	0
35	295	0.447	120	0.148	0.193	0.6	2.113	0.9	0.079	0.8	0.58	1140	11.5	1153	13.1	1178.4	16.1	1178.4	16.1	97	−3
36	167	0.601	91	0.201	0.031	0.7	0.206	1.9	0.049	1.8	0.36	194.1	2.6	189.9	6.7	138.1	42.5	194.1	2.6	102	2
37	143	0.384	50	0.127	0.049	0.7	0.352	2	0.052	1.9	0.34	311.3	4.2	306.5	10.8	270.2	44.3	311.3	4.2	102	2
38	372	0.474	161	0.162	0.048	0.6	0.342	1.3	0.051	1.2	0.46	303.6	3.5	298.9	6.7	262.7	26.8	303.6	3.5	102	2
39	877	0.465	374	0.147	0.288	0.7	5.184	0.9	0.130	0.6	0.74	1633	19.8	1850	15.9	2103.2	12.7	2103.2	12.7	78	−29
40	176	0.658	105	0.222	0.031	0.8	0.221	1.8	0.051	1.7	0.41	198.9	2.9	202.4	6.8	243.2	39.1	198.9	2.9	98	−2
41	42	0.672	26	0.224	0.099	0.8	0.842	2.1	0.062	2	0.35	606	8.7	620.3	20	672.7	43.3	606.0	8.7	98	−2
42	60	0.527	29	0.195	0.117	0.7	1.047	1.7	0.065	1.6	0.38	713.1	8.9	727.5	18	772.1	34	713.1	8.9	98	−2
43	269	0.509	125	0.169	0.032	0.7	0.224	1.7	0.051	1.6	0.4	202.7	2.8	205.1	6.5	232.1	37.1	202.7	2.8	99	−1
44	208	0.434	87	0.178	0.032	0.8	0.252	2	0.056	1.8	0.43	206.1	3.4	228.2	8	463	39.5	206.1	3.4	90	−11
45	197	0.427	82	0.160	0.033	0.9	0.231	2.1	0.051	1.9	0.4	206.4	3.5	210.7	8	258.4	44.6	206.4	3.5	98	−2
46	396	0.637	244	0.230	0.031	0.7	0.217	1.7	0.050	1.6	0.42	198.8	2.9	199.1	6.3	203.7	36.8	198.8	2.9	100	0
47	597	0.118	68	0.042	0.261	0.7	4.061	1.1	0.113	0.8	0.63	1495	18.5	1646	17.9	1846	16.5	1846.0	16.5	81	−24
48	175	0.4	68	0.141	0.032	0.9	0.216	2.1	0.049	2	0.41	204.6	3.5	198.6	7.7	127.6	46.1	204.6	3.5	103	3
49	161	0.405	63	0.150	0.032	1	0.231	2.2	0.052	1.9	0.45	205.2	3.9	210.9	8.2	274.8	44.3	205.2	3.9	97	−3
50	164	0.503	80	0.188	0.032	0.9	0.222	2.4	0.050	2.2	0.36	204.6	3.4	203.6	8.8	192	51.6	204.6	3.4	100	0
51	213	0.951	196	0.344	0.040	0.8	0.270	2	0.050	1.8	0.41	250.1	4	243	8.5	174.8	41.8	250.1	4.0	103	3
52	221	0.431	92	0.161	0.032	0.8	0.228	2.1	0.052	2	0.37	203.5	3.2	208.9	8.1	270.6	45.9	203.5	3.2	97	−3
53	238	0.689	159	0.259	0.033	0.8	0.231	2.2	0.051	2.1	0.34	207.5	3.1	211.2	8.5	253	48.2	207.5	3.1	98	−2
54	85	0.448	37	0.171	0.032	1.3	0.231	3.6	0.052	3.4	0.36	204.2	5.3	211.4	14	292.3	77.9	204.2	5.3	97	−4
55	310	0.541	162	0.195	0.032	0.8	0.231	1.7	0.053	1.5	0.46	201.2	3.2	211.3	6.7	325.8	35.5	201.2	3.2	95	−5
56	442	0.205	88	0.073	0.106	0.7	0.879	1.2	0.060	1	0.59	646.8	8.5	640.5	11.2	618.2	21.2	646.8	8.5	101	1
57	226	0.737	160	0.261	0.032	0.8	0.221	2.1	0.050	1.9	0.4	203.3	3.3	202.9	7.7	198.3	44.7	203.3	3.3	100	0
58	162	0.473	74	0.174	0.031	0.8	0.218	2.3	0.051	2.1	0.34	196.6	3	200.1	8.3	240.9	49.6	196.6	3.0	98	−2
59	113	0.47	52	0.190	0.027	1	0.224	2.8	0.059	2.7	0.33	174	3.3	205.1	10.6	579.9	58.5	174.0	3.3	85	−18

Table. (Continued).

60	193	0.455	85	0.163	0.032	0.9	0.218	2.4	0.049	2.2	0.36	203.7	3.5	199.8	8.7	155	52.2	203.7	3.5	102	2
61	223	0.292	63	0.096	0.345	0.7	5.709	1.1	0.120	0.9	0.62	1913	23.1	1933	19.6	1954.5	16.9	1954.5	16.9	98	−2
62	153	0.494	73	0.179	0.032	0.9	0.215	2.2	0.049	2	0.4	203.4	3.5	197.7	8	130.8	48	203.4	3.5	103	3
63	289	0.662	186	0.242	0.032	0.8	0.234	1.6	0.053	1.4	0.47	204.5	3	213.9	6.2	318.5	32.6	204.5	3.0	96	−5
64	469	0.585	266	0.215	0.042	0.7	0.307	1.5	0.052	1.3	0.48	267.6	3.9	271.7	7.4	306.7	31.1	267.6	3.9	98	−2
65	122	0.46	55	0.162	0.032	1	0.224	2.7	0.051	2.5	0.36	202.5	3.9	204.8	10	231.1	57.8	202.5	3.9	99	−1
66	197	0.433	82	0.163	0.032	0.9	0.234	2.2	0.053	2	0.42	204.4	3.7	213.5	8.5	316.1	45.7	204.4	3.7	96	−4
67	139	0.45	61	0.163	0.032	1	0.227	2.6	0.051	2.4	0.39	205.2	4.1	208.1	9.8	240.9	55.3	205.2	4.1	99	−1
68	118	0.45	52	0.165	0.032	0.9	0.227	2.8	0.052	2.6	0.34	202.7	3.8	207.6	10.4	264.7	59.7	202.7	3.8	98	−2
69	261	0.443	112	0.162	0.031	0.8	0.210	1.9	0.050	1.7	0.41	194.6	2.9	193.2	6.6	176.1	39.8	194.6	2.9	101	1
70	878	1.008	858	0.379	0.052	0.7	0.382	1.2	0.054	1	0.58	323.8	4.4	328.7	6.7	363.6	22.4	323.8	4.4	99	−2
71	206	0.421	84	0.160	0.033	0.9	0.232	2.1	0.051	1.9	0.42	209.5	3.6	211.8	7.9	237.4	43.3	209.5	3.6	99	−1
72	392	0.492	188	0.181	0.033	0.7	0.226	1.5	0.050	1.3	0.48	207.4	2.9	206.6	5.6	196.8	31	207.4	2.9	100	0
73	324	0.432	136	0.160	0.031	0.8	0.211	1.9	0.050	1.7	0.4	194.1	2.9	194	6.6	193.4	40	194.1	2.9	100	0
74	251	0.684	166	0.253	0.032	0.8	0.222	2.1	0.050	2	0.37	204.3	3.1	203.7	7.8	195.8	46.1	204.3	3.1	100	0
75	188	0.483	88	0.178	0.033	0.8	0.238	2.4	0.052	2.3	0.34	209.5	3.4	216.8	9.5	296.7	52.1	209.5	3.4	97	−3
76	290	0.528	148	0.217	0.032	0.7	0.254	2.4	0.058	2.2	0.32	201.4	2.9	230.1	9.7	534.2	49.2	201.4	2.9	88	−14
77	237	0.412	95	0.151	0.031	0.8	0.210	2	0.050	1.8	0.41	194.2	3.1	193.3	7.1	182.1	42.8	194.2	3.1	100	0
78	407	0.695	275	0.255	0.032	0.8	0.219	1.9	0.050	1.8	0.42	203.4	3.2	200.9	7	171.4	41.1	203.4	3.2	101	1
79	264	0.676	173	0.240	0.031	0.7	0.217	1.9	0.050	1.8	0.38	198.5	2.8	199.8	7	214.4	41.3	198.5	2.8	99	−1
80	284	0.397	109	0.151	0.032	0.9	0.236	2.3	0.053	2.1	0.41	205.9	3.8	215.1	8.8	317	47.1	205.9	3.8	96	−4
81	139	0.418	56	0.152	0.032	0.9	0.225	2.6	0.051	2.4	0.35	204	3.7	205.8	9.7	226.2	56.3	204.0	3.7	99	−1
82	157	0.566	86	0.202	0.057	0.9	0.423	1.8	0.053	1.6	0.47	359.9	6	358.4	11.1	348.6	36.8	359.9	6.0	100	0
83	89	0.415	36	0.152	0.050	0.9	0.351	2.2	0.051	2	0.43	312	5.7	305.6	11.5	256.7	45.5	312.0	5.7	102	2
84	146	1.85	262	0.675	0.092	0.9	0.744	1.6	0.058	1.3	0.55	569.8	9.5	564.6	13.6	544	28.9	569.8	9.5	101	1
85	837	0.26	211	0.096	0.039	0.7	0.275	1.3	0.052	1.1	0.55	245	3.4	247	5.6	265.9	24.9	245.0	3.4	99	−1
86	70	0.578	39	0.213	0.032	1.1	0.214	3.3	0.049	3.2	0.34	200.7	4.5	196.9	12	151.8	74	200.7	4.5	102	2
87	208	0.445	90	0.162	0.032	0.8	0.218	2.1	0.049	1.9	0.37	203.3	3.1	200.3	7.5	165.8	45	203.3	3.1	101	1
88	53	0.306	16	0.110	0.072	0.9	0.544	2.4	0.055	2.3	0.37	448.5	7.7	440.8	17.4	400.6	50.7	448.5	7.7	102	2
89	261	0.722	183	0.258	0.032	0.8	0.217	1.8	0.050	1.6	0.45	201.8	3.1	199.7	6.4	174.2	36.8	201.8	3.1	101	1
90	104	0.609	62	0.226	0.032	1	0.206	2.8	0.048	2.7	0.35	200.1	3.9	190.6	9.9	74.9	63.4	200.1	3.9	105	5
91	133	0.466	60	0.170	0.032	0.9	0.215	2.3	0.049	2.1	0.4	202.8	3.7	197.7	8.2	136.9	49.1	202.8	3.7	103	3

Table. (Continued).

Sample_R-4093 (UTM: 37T 0482568E, 4439006N)																				
1	161	0.411	60	0.138	0.026	0.7	0.178	2.4	0.049	2.3	0.29	168.4	2.3	166.8	7.3	143.7	53.7	168.4	2.3	101	1
2	105	0.475	45	0.166	0.032	0.8	0.207	2.4	0.047	2.2	0.36	204.2	3.4	191.2	8.2	33.6	52.8	204.2	3.4	107	6
3	197	0.202	36	0.077	0.032	0.7	0.222	1.9	0.050	1.8	0.36	205.8	2.7	203.9	7	182	41.3	205.8	2.7	101	1
4	177	0.441	71	0.149	0.027	0.7	0.182	2.5	0.049	2.3	0.3	171.5	2.5	169.8	7.7	146.7	55.2	171.5	2.5	101	1
5	298	0.65	177	0.229	0.025	0.7	0.169	1.6	0.049	1.5	0.42	160.8	2.2	158.5	4.8	124.8	34.8	160.8	2.2	101	1
6	166	0.538	81	0.188	0.026	0.7	0.171	2.4	0.048	2.3	0.31	164.1	2.4	159.9	7.2	98.8	55.1	164.1	2.4	103	3
7	499	0.637	289	0.228	0.025	0.6	0.188	1.6	0.055	1.5	0.38	159.5	1.9	175.3	5.2	393.3	34	159.5	1.9	91	–10
8	570	0.439	228	0.153	0.026	0.5	0.175	1.2	0.050	1.1	0.43	163.5	1.7	164	3.7	172.3	26.2	163.5	1.7	100	0
9	142	0.797	103	0.266	0.026	0.8	0.172	2.1	0.049	2	0.36	163.5	2.4	161.5	6.3	133.1	46.7	163.5	2.4	101	1
10	468	0.372	159	0.129	0.026	0.6	0.178	1.5	0.050	1.4	0.36	164.7	1.8	165.9	4.7	183.8	33.6	164.7	1.8	99	–1
11	522	0.421	200	0.146	0.025	0.6	0.170	1.6	0.049	1.4	0.39	161	1.9	159.5	4.6	138.1	34	161.0	1.9	101	1
12	102	0.365	34	0.130	0.032	0.8	0.226	2.1	0.052	2	0.38	200.9	3.2	206.9	8	274.8	45.2	200.9	3.2	97	–3
13	341	0.662	206	0.228	0.049	0.6	0.357	1.2	0.053	1.1	0.45	310	3.4	310	6.5	310.1	25.2	310.0	3.4	100	0
14	308	0.679	191	0.237	0.025	0.6	0.169	1.8	0.048	1.7	0.33	160.8	1.9	158.3	5.2	121.4	39.5	160.8	1.9	102	2
15	129	0.492	58	0.164	0.027	1	0.189	2.7	0.051	2.5	0.38	171.1	3.5	176	8.8	242	57.7	171.1	3.5	97	–3
16	95	0.499	43	0.167	0.027	0.8	0.175	3.1	0.048	3	0.27	170	2.8	164.2	9.5	80.4	71.5	170.0	2.8	104	3
17	159	0.401	58	0.134	0.027	0.7	0.189	2.4	0.050	2.3	0.29	173.4	2.4	176.1	7.7	213.5	52.9	173.4	2.4	98	–2
18	203	0.384	71	0.131	0.027	0.7	0.184	2.2	0.050	2.1	0.31	171.2	2.3	171.6	7	177.2	49.3	171.2	2.3	100	0
19	45	0.974	40	0.324	0.271	0.7	4.088	1.2	0.109	1	0.59	1548	19.5	1652	19.7	1786.6	18.7	1786.6	18.7	87	–15
20	82	0.501	38	0.157	0.037	0.8	0.248	2.2	0.049	2	0.36	232.1	3.6	225.3	8.9	155.7	48.1	232.1	3.6	103	3
21	391	0.613	219	0.195	0.025	0.6	0.179	1.5	0.052	1.4	0.38	160.3	1.8	167.3	4.7	268.7	32.4	160.3	1.8	96	–4
22	499	0.561	255	0.195	0.025	0.6	0.173	1.5	0.049	1.3	0.42	161.9	1.9	162.3	4.4	168.3	31.1	161.9	1.9	100	0
23	60	0.574	31	0.191	0.026	1.1	0.170	3.7	0.047	3.6	0.29	165.1	3.6	159.1	11	71	84.8	165.1	3.6	104	4
24	64	1.723	101	0.576	0.095	0.7	0.770	1.7	0.059	1.5	0.42	582.8	7.8	579.9	14.9	568.7	33.5	582.8	7.8	101	0
25	773	0.503	356	0.172	0.048	0.5	0.354	1	0.054	0.9	0.52	302.3	3.1	307.9	5.3	350.7	19.9	302.3	3.1	98	–2
26	148	0.477	64	0.162	0.026	0.8	0.179	2.6	0.050	2.4	0.31	166.1	2.6	166.9	7.9	177.3	56.8	166.1	2.6	100	0
27	99	0.83	80	0.298	0.030	0.9	0.199	2.8	0.047	2.6	0.34	192.9	3.6	183.9	9.3	70.6	61.6	192.9	3.6	105	5
28	518	0.407	193	0.139	0.026	0.7	0.177	1.5	0.050	1.3	0.45	162.5	2.1	165.6	4.5	209.9	30.9	162.5	2.1	98	–2
29	554	0.765	389	0.266	0.024	0.6	0.164	1.4	0.049	1.3	0.42	155.9	1.8	154.5	4.1	133.7	30.7	155.9	1.8	101	1
30	96	0.575	50	0.199	0.026	0.9	0.181	2.7	0.050	2.5	0.34	168.1	3	169.1	8.3	181.9	58.2	168.1	3.0	99	–1
31	137	0.555	69	0.182	0.026	0.8	0.175	2.3	0.049	2.1	0.37	163.6	2.7	163.6	6.8	163.6	49.2	163.6	2.7	100	0

Table. (Continued).

32	165	0.46	69	0.158	0.027	0.8	0.183	1.8	0.049	1.7	0.43	172.6	2.7	170.4	5.7	139.8	39.1	172.6	2.7	101	1
33	86	0.894	70	0.306	0.025	1	0.179	3	0.052	2.9	0.32	160.2	3	167.5	9.4	273	65.9	160.2	3.0	96	−5
34	119	0.623	68	0.201	0.025	1	0.169	2.5	0.048	2.3	0.38	161.8	3	158.2	7.3	103.4	54.6	161.8	3.0	102	2
35	120	1.498	164	0.510	0.073	0.6	0.571	1.5	0.057	1.4	0.42	455.5	5.5	458.8	11	475.6	30.3	455.5	5.5	99	−1
36	368	0.313	105	0.113	0.051	0.6	0.366	1.2	0.052	1.1	0.45	319	3.4	316.6	6.7	298.7	25.7	319.0	3.4	101	1
37	165	0.494	74	0.169	0.032	0.8	0.219	2.3	0.050	2.1	0.36	201.6	3.2	201.2	8.3	196.3	49.8	201.6	3.2	100	0
38	137	0.48	60	0.170	0.026	0.8	0.192	2.5	0.054	2.4	0.31	165	2.5	178.5	8.3	361.3	54.2	165.0	2.5	92	−8
39	206	0.444	83	0.154	0.027	0.7	0.185	2.1	0.050	2	0.32	170	2.3	172.2	6.6	202.6	45.8	170.0	2.3	99	−1
40	128	0.508	59	0.173	0.026	0.8	0.172	2.8	0.049	2.7	0.29	163.7	2.6	161.2	8.3	125.5	63	163.7	2.6	102	2
41	478	0.69	300	0.234	0.050	0.5	0.368	1.1	0.054	1	0.47	313.6	3.3	318.3	6.2	352.5	23.2	313.6	3.3	99	−1
42	166	0.622	95	0.177	0.339	0.6	5.935	0.9	0.127	0.7	0.6	1880	18.5	1966	16.4	2059.1	14.6	2059.1	14.6	91	−10
43	185	0.861	147	0.301	0.025	0.7	0.170	2	0.050	1.9	0.35	158.7	2.2	159.8	6	176	44.5	158.7	2.2	99	−1
44	139	0.373	47	0.122	0.026	0.8	0.166	2.6	0.046	2.5	0.33	164.9	2.8	155.8	7.5	20	59	164.9	2.8	106	6
45	714	0.065	42	0.017	0.069	0.5	0.544	1	0.057	0.8	0.54	431.1	4.5	441.2	7.1	494.5	19	431.1	4.5	98	−2
46	208	0.439	83	0.151	0.026	0.7	0.173	1.7	0.047	1.5	0.41	168.1	2.3	161.6	5.1	67.2	37	168.1	2.3	104	4
47	126	0.446	51	0.152	0.048	0.7	0.349	1.7	0.053	1.6	0.39	303.2	4	304.3	9.1	313	36.7	303.2	4.0	100	0
48	654	0.368	220	0.131	0.049	0.6	0.359	1.1	0.053	0.9	0.53	308.5	3.4	311.4	5.7	333	20.9	308.5	3.4	99	−1
49	1780	0.322	522	0.112	0.046	0.6	0.359	1	0.056	0.8	0.58	292.3	3.2	311.4	5.2	456.9	17.9	292.3	3.2	94	−7
50	183	0.404	68	0.143	0.051	0.7	0.380	1.7	0.054	1.5	0.41	320.7	4.3	327.3	9.3	375.1	34.4	320.7	4.3	98	−2
51	167	0.412	63	0.142	0.027	0.8	0.182	2.4	0.050	2.3	0.32	169.1	2.6	169.4	7.6	173.2	53.7	169.1	2.6	100	0
52	46	0.634	26	0.216	0.025	1.3	0.191	4.4	0.055	4.2	0.31	161.4	4.3	177.2	14.3	394.1	93.6	161.4	4.3	91	−10
53	260	0.679	161	0.231	0.049	0.5	0.358	1.4	0.053	1.3	0.37	310.1	3.2	310.7	7.7	314.7	30.7	310.1	3.2	100	0
54	885	0.672	541	0.231	0.049	0.5	0.362	1	0.054	0.9	0.52	307.5	3.2	313.9	5.6	361.5	20.4	307.5	3.2	98	−2
55	191	0.557	142	0.255	0.027	1.5	0.264	3.2	0.070	2.8	0.47	173	5	237.5	13.4	936	57.4	173.0	5.0	73	−37
56	180	0.653	147	0.221	0.073	1.4	0.696	1.9	0.069	1.3	0.73	455.6	12	536.2	15.6	895.9	26.8	455.6	12.0	85	−18
57	116	0.615	95	0.227	0.026	1.6	0.182	2.8	0.051	2.4	0.55	165.2	5.1	169.9	8.9	235.9	55.2	165.2	5.1	97	−3
58	331	0.491	217	0.180	0.049	1.4	0.368	1.9	0.054	1.2	0.75	310.6	8.4	318	10.1	372.7	28.1	310.6	8.4	98	−2
59	391	0.272	143	0.101	0.050	1.4	0.364	1.9	0.053	1.2	0.74	315.1	8.4	314.9	10	313.2	28.7	315.1	8.4	100	0
60	221	0.871	264	0.455	0.029	1.4	0.415	2.3	0.105	1.9	0.61	182.4	5.1	352.3	14	1710.5	34.9	182.4	5.1	52	−93
61	228	0.376	114	0.139	0.051	1.4	0.368	1.9	0.053	1.4	0.7	317.8	8.4	318.1	10.6	320.3	31.8	317.8	8.4	100	0
62	146	0.68	133	0.244	0.027	1.4	0.190	2.6	0.052	2.2	0.55	168.7	4.7	176.7	8.4	285.1	49.4	168.7	4.7	95	−5
63	123	0.505	83	0.162	0.025	1.4	0.170	2.7	0.050	2.3	0.53	158	4.5	159.4	7.9	179.8	53	158.0	4.5	99	−1

Table. (Continued).

64	257	0.543	174	0.152	0.051	1.4	0.396	1.9	0.056	1.3	0.72	322.3	8.5	338.6	10.9	452.4	29.3	322.3	8.5	95	–5
65	1043	0.246	346	0.089	0.047	1.4	0.355	1.7	0.055	1	0.79	297.2	7.9	308.6	9.1	395.3	23.6	297.2	7.9	96	–4
66	380	0.306	155	0.111	0.052	1.3	0.380	1.8	0.053	1.1	0.76	327.1	8.5	327.2	9.8	328.4	26.3	327.1	8.5	100	0
67	806	0.563	610	0.186	0.042	1.3	0.340	1.7	0.059	1.1	0.77	264.9	6.9	296.9	8.8	556.8	24.3	264.9	6.9	89	–12
68	1276	0.243	413	0.081	0.048	1.3	0.370	1.7	0.056	1	0.79	303	7.8	319.4	9.1	440.9	23	303.0	7.8	95	–5
69	223	0.375	111	0.136	0.027	1.4	0.186	2.1	0.050	1.6	0.65	171.5	4.6	173.2	6.6	196.5	36.9	171.5	4.6	99	–1
70	66	0.593	52	0.186	0.026	1.5	0.201	3.2	0.056	2.8	0.48	166.1	5	185.7	10.9	443	62.9	166.1	5.0	89	–12
71	107	0.415	59	0.152	0.027	1.5	0.178	2.8	0.048	2.4	0.52	171.5	4.9	166.2	8.6	90.8	57.1	171.5	4.9	103	3
72	71	0.688	66	0.252	0.027	1.5	0.176	3.1	0.048	2.6	0.5	169.7	5.1	165	9.3	98.5	62.5	169.7	5.1	103	3
73	1159	0.449	684	0.159	0.038	1.5	0.296	1.9	0.057	1.1	0.79	237.6	6.8	263.5	8.6	500.1	25.6	237.6	6.8	90	–11
74	146	0.566	113	0.202	0.028	1.4	0.183	2.3	0.047	1.9	0.6	178.7	4.9	170.4	7.3	57.4	44.8	178.7	4.9	105	5
75	83	0.455	50	0.168	0.030	1.4	0.205	3	0.050	2.6	0.48	190.2	5.4	189.7	10.4	184.5	61.5	190.2	5.4	100	0
76	435	0.87	504	0.319	0.025	1.4	0.171	2	0.049	1.4	0.7	161	4.4	159.9	5.9	143.3	33.3	161.0	4.4	101	1
77	202	0.616	169	0.235	0.026	1.4	0.185	2.5	0.051	2.1	0.56	166.7	4.6	172.6	7.9	255.5	47.4	166.7	4.6	97	–4
78	423	0.626	355	0.244	0.027	1.4	0.216	1.9	0.058	1.3	0.74	171.3	4.7	198.4	6.8	534	28.3	171.3	4.7	86	–16
79	65	0.427	37	0.155	0.027	1.5	0.172	3.3	0.046	2.9	0.45	171.8	5	161	9.8	4.3	69.6	171.8	5.0	107	6
80	63	0.559	47	0.181	0.026	1.6	0.178	3.4	0.050	3.1	0.45	165.6	5.1	166.2	10.5	174.5	71.5	165.6	5.1	100	0
81	579	0.461	357	0.171	0.026	1.3	0.175	1.9	0.049	1.4	0.69	164.5	4.3	164.1	5.8	158.5	32.7	164.5	4.3	100	0
82	300	0.517	208	0.193	0.050	1.4	0.394	1.9	0.057	1.3	0.72	314.3	8.5	337.1	11	497.5	29.3	314.3	8.5	93	–7
83	550	0.381	281	0.137	0.048	1.3	0.349	1.7	0.053	1.1	0.76	299.4	7.7	303.8	9.1	337.9	25.7	299.4	7.7	99	–1
84	302	0.338	136	0.127	0.026	1.3	0.177	2	0.049	1.4	0.69	165.1	4.4	165.1	6	164.4	33.6	165.1	4.4	100	0
85	144	0.33	63	0.127	0.051	1.3	0.385	2.2	0.055	1.8	0.61	320.8	8.4	331	12.5	403.4	39.6	320.8	8.4	97	–3
86	67	0.579	52	0.218	0.025	1.7	0.173	3.5	0.050	3.1	0.47	161.4	5.3	162.1	10.6	172	72.8	161.4	5.3	100	0
87	35	0.366	17	0.130	0.032	1.7	0.218	3.8	0.049	3.4	0.44	205.5	6.7	200.2	13.7	137.8	79.6	205.5	6.7	103	3
88	107	0.481	69	0.173	0.025	1.5	0.177	2.9	0.051	2.4	0.53	161.1	4.8	165.3	8.8	225.7	56.7	161.1	4.8	97	–3
89	80	0.425	45	0.161	0.027	1.5	0.195	2.9	0.052	2.5	0.52	171.7	5	180.7	9.5	300.1	56.3	171.7	5.0	95	–5

* $^{206}Pb/^{238}U$ ages are used when ages are <1.0 Ga, whereas $^{207}Pb/^{206}Pb$ ages are used when ages are >1.0 Ga.

**Concordance rate calculated as $^{206}Pb/^{238}U$ ages divided by $^{207}Pb/^{235}U$ ages when ages are <1.0 Ga and $^{206}Pb/^{238}U$ ages divided by $^{207}Pb/^{206}Pb$ ages when ages are >1.0 Ga.

#Discordance rate calculated using the formula (1 – [($^{207}Pb/^{235}U$ date) / ($^{206}Pb/^{238}U$ date)] × 100 when ages are <1.0 Ga and (1 – [($^{207}Pb/^{206}Pb$ date) / (^{206}Pb /^{238}U date)]) × 100 when ages are >1.0 Ga.